DETechnologies Hydrogen-Oxygen Rotating Detonation Rocket Engine Development

Final Report: ME 8705 - Mechanical Engineering Capstone II
Memorial University of Newfoundland and Labrador

Miri, Shakib	Palmer, Logan	Clark, Aidan	Cleary, Patrick
smiri@mun.ca	lrpalmer@mun.ca	amhclark@mun.ca	pcleary@mun.ca
201848900	201906765	201919990	201901261

Academic Supervisor:
Dr. Xili Duan
xduan@mun.ca

05 April 2024

Abstract

This paper is the culmination of a 16-month capstone project at Memorial University of Newfoundland, Faculty of Engineering and Applied Sciences. The goal of this project was to develop a model to design an Rotating Detonation Engine using currently published research to help address a noted research gap. It was also sought to produce a prototype for hot-fire testing. The analytical model developed in MatLab drew on first-principles formulations from literature and toolbox plugins. This model resulted in a detonation cell size of 1.2mm, maximum temperature of 3720K, maximum pressure of 4.3MPa, mass flow rate of 334g/s, specific impulse of 410.7s, area ratio of 5.45% at a plenum pressure of 1.102MPa for Hydrogen feeding, area ratio of 12.27% at a plenum pressure of 0.9757MPa for Oxygen feeding given a target thrust of 1350N, input pressure of 130kPa, input temperature of 300K, equivalence ratio of 1, propellant mixture of GH2-GO2, and a fill height of 37.5mm. The combustion chamber has an outer diameter of 60mm, an inner diameter of 50mm, a channel width of 5mm, and a length of 50mm. Finite Element Analysis is performed to determine mode shapes, static thermal and pressure analysis using Altair HyperMesh and the OptiStruct solver. The mesh is primarily formed from first-order hexahedral elements with minimal amounts of first-order pentahedral elements. To represent the 316L-SS material, a linear isotropic material model was selected. Given the calculated wave frequency of 16.4937kHz, the modal analysis determined that this was within 5Hz of the 40th mode of the engine. The static thermal determined a maximum thermal stress of 38GPa, proving that this RDE could not be run to steady conditions. The static pressure results provided a maximum stress of 16.32MPa, which is well below the yield strength of 316L stainless steel. The two CFD simulations were developed using the Convergent Science software CONVERGE CFD. The 2D stoichiometric Hydrogen and Oxygen combustion simulation currently shows promising results, but is not yet a fully functional model. The 3D non-reactive flow model is built to ensure propellant injection choking and mixing. Choked flow is confirmed in the fuel/oxidizer injectors but the model shows poor mixing due to supersonic propellant entry speeds. The engine is made up of 4 parts, the base plate, injector plate, outer body, and center body. Alignment between the center body and the outer body bore is critical for a concentric annular combustion chamber. A maximum of 117 microns of misalignment between the centre body OD and outer body bore can exist. Nitrile O-Rings are used for sealing between the components. Some future work can occur on this project; Re-design the combustion chamber structure to avoid operating near resonant frequencies, improve the analytical model to include design point calculation above the minima and consider system losses, perform cold-flow testing of individual components, and have a prototype fabricated for hot-fire testing.

Acknowledgements

Thank-you to everyone who has supported our team over the past 16 months during our senior capstone design project. A special thank-you to Dr. X. Duan for being our capstone academic supervisor and working with us to prove there is value in 2-term capstone projects within the Mechanical Engineering Department at Memorial University of Newfoundland. While not being an RDE researcher, you've still assisted us technically and have encouraged us to keep progressing despite numerous roadblocks. Without your approval to oversee this project, we would have never been able to start this journey.

To the international technical experts Dr. Q. Michalski (Royal Melbourne Institute of Technology), Dr. Craig Nordeen, Dr. J-P. Hickey (University of Waterloo), Dr. J. E. Shepherd (California Institute of Technology), Dr. A. Higgins (McGill University), Dr. C. Kiyanda and S. Connolley-Boutin (Concordia University), we thank you for sharing what information you could regarding the complexities of turbulence, combustion, detonation, and RDEs to help guide us towards solutions to our early-stage problems and answer questions not found in a paper. Our discussions have led to overcoming roadblocks thought impossible and allowed for the continued progression of our work.

Thank-you to Dr. S. Nakhla, Dr. A. Elruby, Dr. S. Bruneau, K. Hong (Memorial University of Newfoundland) for pushing us technically, and for supporting our work in various incredibly important capacities much of this work would not be possible without your support.

Thank-you to L. Heath for agreeing to spend your second Engineering work-term with our team. You are incredibly hard-working and have far exceeded our expectations in every aspect of your work-term. We hope you've enjoyed this learning experience as much as we have.

A broad thank-you to the following folks who have provided some sort of support, assistance our guidance during various stages of the project thus far. E. Martin, P. White, T. Hart, Dr. G. Rideout, S. Noseworthy, Dr. C. Bazan, J. Stevens, R. Meany, J. Walsh, S. March, J. Conway, M. Quinn, K. Chirke, N. Shukla, D. Kirkpatrick, T. Ricketts, A. Keating, H. Leystra, A. Trumpour, A. Campbell, M. Coombs, K. Whelan.

Contents

List of Figures

List of Tables

List of Equations

1 Introduction and Background

1.1 Topic Introduction

A Rotating Detonation Engine (RDE) is a novel rocket engine operating on the principle of detonation, or supersonic combustion. Detonation is a highly efficient mode of combustion with applications in astronautical, aeronautical, and defence industries. Peak theoretical efficiency gains of detonation combustion compared to traditional sub-sonic combustion ranges between 10% and 25% [1]. While detonation engine technology is very immature, existing only in the research industry, harnessing the power of detonation is not a new concept. Early groundwork for a RDE was established by Voitsekhovskii in 1959 [2] with a continuous gas detonation process in a toroidal combustion chamber [3]. Detonation as a mode of combustion is inherently difficult to control, plaguing rocket engine development, like the Apollo F1 program [4], [5] . In the past 10-20 years there has been a significant spike in interest to develop a new high power, high efficiency propulsion method to support a renewed interest in space exploration, and hyper-sonic travel.

1.2 Project Scope

The scope of this project is to develop a procedure to size a Rotating Detonation Engine, validate sizing results using numerical methods, and to prepare the engine for fabrication.

While not in the core scope of this project, additional sections are included in this report which outline basic, but necessary, initial steps to size a propellant feed system, engine ignition system, and conceptual design of a thrust stand for laboratory characterization of engine performance. Each of these are crucial to the operation of the final product, hence the constraints implied by each system on the engine must be well understood.

1.3 Problem Formulation

Sizing of a Rotating Detonation Engine for specific applications is not well defined, owing to the immature nature of the technology, and understanding of controlling the detonation phenomena. To address the industry research gap, the goal of this project is to undertake an analytical approach to sizing a basic RDE for application in a research environment.

1.4 Constraints

Constraints defining the design direction are broken down into technical and non-technical in the following two sub-sections.

1.4.1 Non-Technical

Timeline: The timeline for this project is constrained to 16 months, having taken initiative to begin this project in January of 2023. The timeline for this project is further constrained by two work-terms, and two academic semesters during this 16-month period.

Monetary: Monetary constraints for this project, outlined by Memorial University of Newfoundland, Faculty of Engineering and Applied Science, Department of Mechanical Engineering, stipulates that cost-matching can be provided for student capstone projects, up to the total amount of $500. Additional costs are to be sole-funded by the capstone team members, and/or industry partners.

Testing Facilities: Approved laboratory facilities are not readily available in Newfoundland, nor Atlantic Canada. Design testing is therefore limited to private testing, without the knowledge of MUN representatives.

1.4.2 Technical

Safety: Safety is the number one constraint on this project, whether testing is conducted or not, suitable factors of safety are applied.

Maximum Pressure: Upstream pressures are limited by the intended propellant storage source: standard size 44 compressed gas canisters which are stored at 2200 psi. A qualitative constraint is applied to minimize upstream pressure, to limit severity of catastrophic failure.

Maximum Prolonged Temperature: Due to the nature of detonation combustion, and the selected propellant, flash temperatures exceed the melting temperature of available materials. Understanding this, maximum run-times of the design engine are limited to ¡2 seconds to ensure engine does not approach melting temperatures.

Engine Materials: Engine construction materials are limited to what is readily available for manufacturing in Atlantic Canada for use with traditional manufacturing processes.

Manufacturing Processes: Manufacturing processes are constrained to traditional subtractive manufacturing tools, which can be found in most modern machine shops. This constraint is imposed to limit design complexity, ensuring that a standard machine shop is able to manufacture engine components.

Thrust Target: The designed thrust target for this engine, operating in single-wave mode, on Hydrogen and Oxygen propellant is 1350N.

2 Literature Review

2.1 Combustion Processes

Most combustion engines can be approximated by the Brayton cycle, an isobaric combustion process. Detonation combustion cycles are approximated by the Humphrey or Fickett-Jacobs cycles. The Humphrey cycle is an ideal isochoric, or pressure gain, combustion cycle, whereas the Fickett-Jacobs cycle is a similar, pressure gain combustion cycle, modeled to more closely represent the physical detonation process. Efficiency gains of isochoric combustion cycles compared to isobaric combustion are easily seen from their respective Pressure-Volume (PV) curves. PV curves of Brayton (isobaric), Humphrey (isochoric), and Fickett-Jacobs (isochoric) cycles are shown in Figure 1.

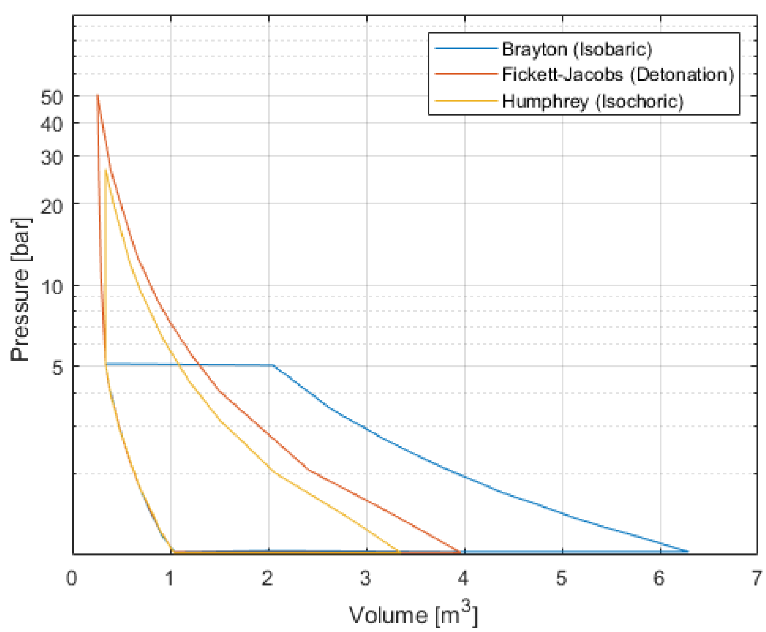

Figure 1: PV Diagram for Brayton, Humphrey, Fickett-Jacobs Cycles, adapted from Wolański [6]

In each of the four cycles depicted in Figure 1, the process between each numerical state can be generalized as follows.

- $1 \rightarrow 2$: Compression.
- $2 \rightarrow 3$: Combustion.
- $3 \rightarrow 4$: Expansion.

- 4 → 1 : Compression (via cooling).

The difference between Isochoric and Isobaric combustion is shown in the combustion stages between states 2→3. Notice the constant pressure line between states 2 and 3 of the Brayton cycle, compared to the constant volume process between states 2 and 3' and 3" of the Humphrey and Fickett-Jacobs cycles, respectively. Since the area under the PV curve is representative of the efficiency of the cycle, it is straightforward to visually see how the high peak of the isochoric combustion cycles contributes to the overall higher efficiency of detonation cycles. Theoretical cycle efficiencies for stoichiometric combustion of hydrogen and air for each of these three cycles are shown in Table 1 according to [1].

Table 1: Combustion Cycle Efficiencies for Stoichiometric Combustion Between Hydrogen and Air [1]

Reactants	**Brayton [%]**	**Humphrey [%]**	**Fickett-Jacobs [%]**
Hydrogen & Air at ϕ =1.00	36.9	54.3	59.3
Acetylene (C_2H_2) & Air at ϕ=1.00	36.9	54.1	61.4

2.2 Detonation Combustion

The first widely accepted theory which attempts to describe detonation combustion is the Chapman-Jouguet (CJ) theory, which is a synthesis of Chapman [7] and Jouguet [8] zero-th dimensional approximation of properties across a detonation wave front. These theories attempt to describe the relation between thermochemical properties of reactants and products across a detonation wave. Kuo [9] presents a full derivation of the Rankine-Hugoniot relation from the conservation equations shown in Equations 1 through 3 [9]. The Hugoniot relation, shown in Equation 4, describes the solutions for all downstream pressure, p_2 and specific volume, $\nu = \frac{1}{\rho_2}$, given initial conditions p_1, ρ_1^{-1} and heat of combustion q_{rxn}, if chemical reaction is present.

Continuity.

$$\frac{d(\rho u)}{dx} = 0 \tag{1}$$

Momentum.

$$\rho u \frac{du}{dx} = -\frac{dp}{dx} + \frac{d}{dx}[(\frac{4}{3}\mu + \mu')\frac{du}{dx}] \tag{2}$$

Energy.

$$\rho u[\frac{d}{dx}(h + \frac{u^2}{2})] = -\frac{d}{dx}q_{cond} + \frac{d}{dx}[u(\frac{4}{3}\mu + \mu')\frac{du}{dx}] \tag{3}$$

Hugoniot Relation

$$\frac{\gamma}{\gamma - 1}(\frac{p_2}{\rho_2} - \frac{p_1}{\rho_1}) - \frac{1}{2}(p_2 - p_1)(\frac{1}{\rho_1} + \frac{1}{\rho_2}) = q_{rxn} \tag{4}$$

Where γ is the ratio of reactant specific heats.

Two critical points identified by the CJ theory are called the upper and lower CJ points, respectively [7][8]. The upper and lower CJ points represent the minimum and maximum points where detonation and deflagration can exist, respectively. Figure 2 described in detail the relation of the CJ points to detonation and deflagration [10]. Understanding where and how the CJ points can be influenced is essential in designing a combustion system to behave as expected, as they are representative of the physical operating conditions in a system.

The Hugoniot curve can be divided into five regions, as shown in Figure 3, where each region represents a different combustion mode. Not all of these combustion modes are physically realizable. Regions of particular interest are I - Strong Detonation and II - Weak Detonation, divided by the upper-Chapman-Jouguet (UCJ) point. The UCJ point is defined by the position at which a line drawn from P_1, ρ_1^{-1} (the Rayleigh Line) is tangent to the Hugoniot curve.

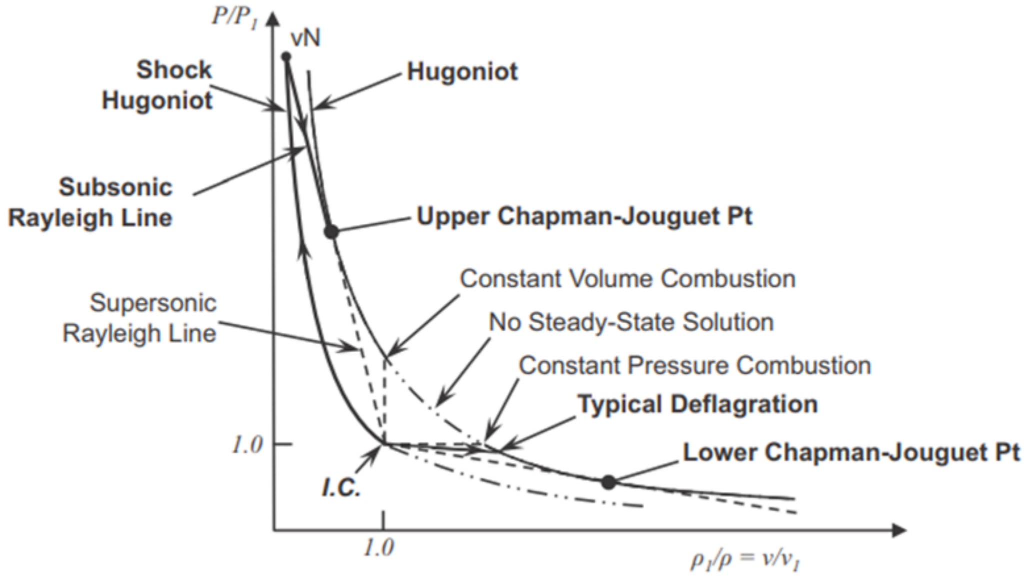

Figure 2: P-V Diagram of Rankine-Hugoniot Curves [10]

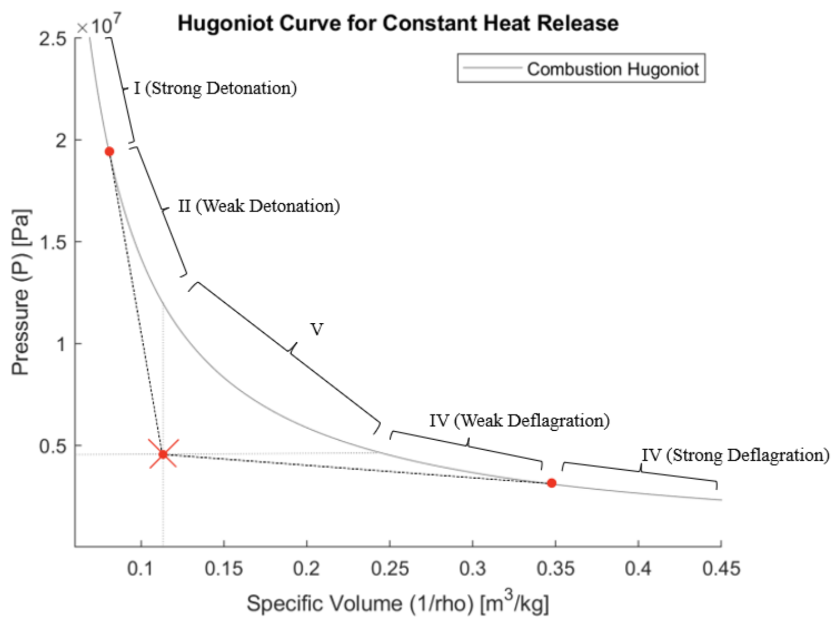

Figure 3: Combustion Regions represented on Hugoniot plot adapted from Kuo [9]

In region I - Strong Detonation, it can be shown that the pressure of the post-combustion gasses is higher than the pressure of the combustion wave itself, $P_2 > P_C$. The detonation wave travels below the speed of sound in this region [9]. This type of detonation is hard to achieve, requiring extreme confinement [9]. Region II - Weak Detonation has a bi-product pressure less than the pressure of the combustion wave $P_2 < P_C$. Gas speed in this region slows down significantly across the combustion wave but still remains above the speed of sound [9]. Weak detonation requires reactants with very high-speed chemical kinetics [9]. The point of specific interest in the design of RDEs is the Upper-CJ point, where combustion bi-products maintain the same pressure as the combustion wave and travel at the speed of sound in the burned gas mixture. The CJ is also the local minima of entropy generation [11]. Because of this minimum of entropy, and the difficult requirements needed to achieve states 1 and 2, if detonation is instigated within states 1 and 2, it will tend towards the Upper CJ point [12].

The Zel'dovich, von Neumann, and Doring (ZND) theory is built upon the Chapman Jouguet theory by Zel'dovich [13], von Neumann [14] and Doring [15]. These theories extend CJ theory by considering the combustion wave as 1D and steady relative to the detonation front. These theories collectively postulate that a detonation wave consists of a leading shock wave that compresses the reactants, thereby increasing the pressure and temperature, followed by a secondary chemical reaction, a combustion wave. The zone in between the leading shock and combustion wave has been termed the induction zone, and no chemical reactions occur. According to these theories, the leading supersonic shock wave compresses the reactants such that the following combustion wave propagates at a subsonic speed relative to the reactants but at a supersonic speed relative to a pre-compression reference frame. The temperature increase from the compression also increases the thermal efficiency of combustion, due to resultant higher combustion temperatures. A ZND representative detonation wave is shown by Kuo [9] in Figure 4.

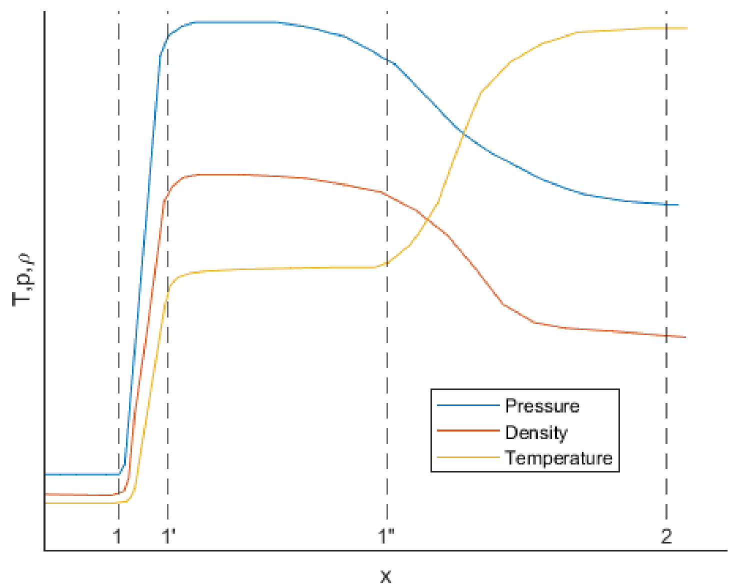

Figure 4: ZND Wave Structure Adapted from Kuo [9]

Figure 4 shows four key points of Temperature T, Pressure P, and Density ρ. Initial properties increase steeply across the width of the leading shock wave from point 1 to 1'. Position 1' is also called the von Neumann spike, the point at which the system reaches its maximum pressure. Within the induction zone, between states 1' and 1", the pressure, temperature, and density all remain roughly constant at the compressed state. At point 1", the mixture reacts; pressure P and density ρ drop, while temperature T increases sharply. As discussed earlier, the decreased product pressure is still higher than the initial reactant pressure, hence the term pressure-gain combustion.

2.3 Types of Detonation Engines

There are two main types of detonation engines; the Pulse Detonation Engine (PDE) and the continuous detonation engine, or Rotating Detonation Engine. Each engine type is discussed separately in their respective subsections.

2.3.1 Pulse Detonation Engines

Pulse Detonation Engines operate cyclically in a fill, fire, purge cycle. The efficiency of these engines is limited by the upper frequency at which this three-stage cycle can occur. PDEs are typically long cylindrical tubes, where fresh propellant is injected on one end, and a spark ignites the mixture [16]. The combustion ensues, in sub-sonic, deflagration mode throughout a distance axially along the tube, accelerating until it exceeds the sonic threshold [16]. The point at which combustion speed reaches Mach = 1, or the transition point from deflagration to detonation, is called the Deflagration-to-Detonation Transition (DDT) point. The axial length at which the DDT occurs is a function of the thermochemical combustion parameters and the confinement of the cylindrical combustion tube. The DDT position can be influenced to increase in less distance using an internal Schelkin spiral geometry. A Schelkin spiral is a helical spiral shape which is commonly used to decrease the distance at which DDT, occurs. Alternative approaches to reducing the DDT distance is by increasing the internal tube wall friction. Typical geometry of a simple PDE, equipped with a Schelkin spiral is borrowed from Li [17] in Figure 6b.

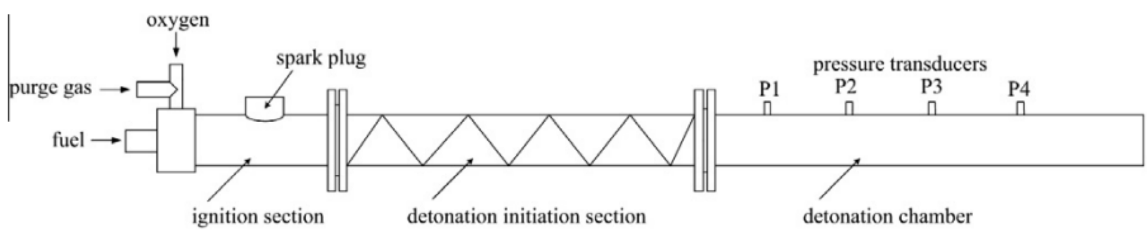

Figure 5: PDE with Schelkin Spiral Schematic from Li [17]

PDEs have been applied to real applications in experimental environments, such as small unmanned rockets [18] and one application of a small aircraft [19].

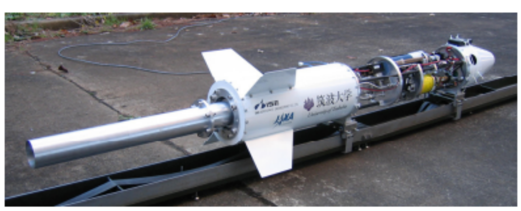

(a) PDE Powered Rocket from Kasahara [18]

(b) First flight powered by a PDE [19]

Figure 6: Experimental PDE Applications

2.3.2 Rotating Detonation Engines

Continuous detonation engines, alternatively known as Rotating Detonation Engine (RDE)s, are not burdened by a cyclic, mechanically driven, combustion process. As the names suggest, continuous detonation engines operate such that a combustion wave continually propagates through the combustion chamber while fresh propellant is continually injected. The combustion wave propagates in the azimuthal direction, with an oblique shock-wave trailing the main combustion front creating thrust in the axial direction. Two schematics depicting this process are shown in Figure 7. These schematics provide a good high-level understanding of the basic combustion propagation mechanisms ongoing within a RDE combustion chamber.

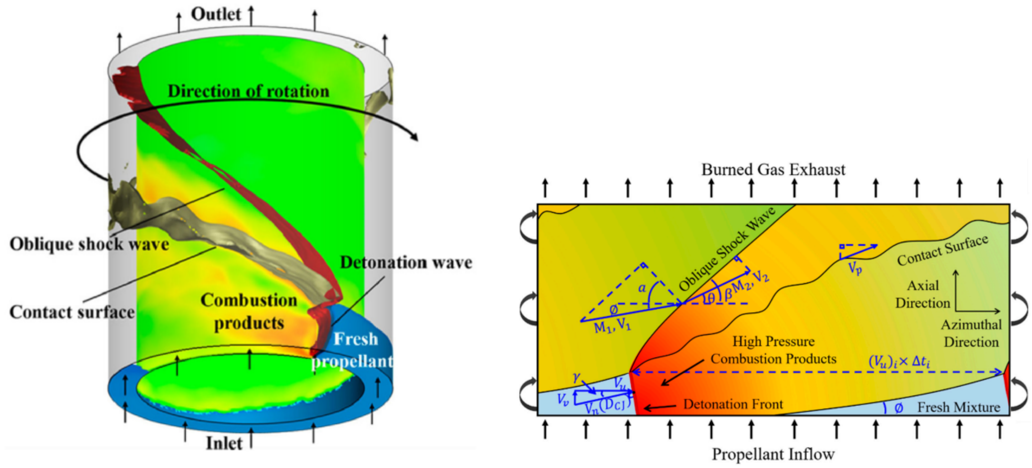

(a) RDE Schematic from Rong [20]

(b) RDE Schematic from Han [21]

Figure 7: RDE Combustion Schematics

A number of organizations have even attempted to equip nozzles and aerospikes on numerical and experimental RDE research work, with varying degrees of success [22] [23] [24].

2.4 Combustion Chamber of Rotating Detonation Engines

Geometric parameters of the RDE can be estimated using detonation cell size, λ, estimates based on [25], [26], [27]. Geometric engine parameters are estimated using rules of thumb from [1], [28], [29], and [30] correlated to detonation cell size estimates, summarized in Table 2.

Table 2: Summary of published Rules of Thumb for RDE Geometry According to Respective Theories

Parameter	Bykovskii [28]	Nair [30]
Minimum Fill Height, h^*	$(12 \pm 5)\lambda$	$(12 \pm 5)\lambda$
Minimum Outer Diameter, D_{min}	28λ	40λ
Minimum Channel Width, δ_{min}	$\frac{h^*}{5}$	2.4λ
Minimum Length, L_{min}	$> 2h$	24λ

2.5 Generating Thrust in a Rotating Detonation Engine

Relating CJ and ZND detonation wave parameters to engine thrust is accomplished by approximating purely mean axial flow from a 2D azimuthal expansion process, as presented by Shepherd in [31]. Using a control volume approach, the net mean azimuthal flow at the exit of the combustion chamber is shown to be zero according to the conservation of angular momentum, evident by Equation 5 [31].

Conservation of angular momentum, M for stationary control volume Ω and control surface $\partial\Omega$ [31].

$$M = \frac{\partial}{\partial t}\int_{\Omega} r \times \rho u dV + \int_{\partial\Omega}(r \times \rho u) n \cdot u dS \tag{5}$$

Where ρ is density, r is the radius, u is velocity vector. Since the control volume surrounding the RDE does not rotate, the first term evaluates to zero [31]. The second term can be re-written considering the geometry of a RDE, a simple annulus cylinder, assuming uniform flow in the radial direction, Equation 6 [31].

$$\frac{1}{2\pi}\int_{0}^{2\pi} \rho(\theta', z)\nu(\theta', z)w(\theta', z)d\theta' = \overline{\rho\nu w} = 0 \tag{6}$$

Where v is azimuthal speed, w is axial speed, θ is angle. Since the average of the azimuthal and axial, accompanied by the net zero angular momentum indicates that $\overline{\nu} << \overline{w}$ [31].

This understanding that pure azimuthal detonation flow within the combustion chamber of a RDE resolving to mean pure axial flow exiting the combustion chamber, allows for specific thrust to be written. For the case of expansion to atmospheric pressure P_a and assuming isentropic expansion along streamlines, Equation 7 is written [31]. Full derivation of specific thrust equation shown by Shepherd in [31].

$$\left.\frac{\tau}{\dot{M}}\right|_{P_a} = w = a_1\sqrt{\frac{2}{\gamma-1}}\left[1+\frac{1}{2(\gamma+1)}\left(M_{CJ}-\frac{1}{M_{CJ}}\right)^2-\left(\frac{P_a}{P_1}\right)^{\frac{\gamma-1}{\gamma}}\frac{1}{M_{CJ}^2}\left(\frac{\gamma+1}{\gamma M_{CJ}^2+1}\right)^{\frac{-(\gamma+1)}{\gamma}}\right]^{\frac{1}{2}} \tag{7}$$

Where P_1 is the initial pressure, P_a is atmospheric pressure, γ is the ratio of specific heats, M_{CJ} is the CJ wave speed mach number. Using CJ detonating wave parameter, the resulting specific thrust can be calculated, allowing detonation wave parameters to be related to RDE performance.

2.6 Ongoing Rotating Detonation Engine Research

Several agencies are researching RDE technology with a variety of propellant types. Some notable RDE researchers are: Wolanski [32], Bykovskii [33], Nordeen [34], Michalski [35], and Connolly-Boutin [36].

There exists a small-scale, non-premixed, gas-gas, Hydrogen and Oxygen propellant RDE that is shared amongst research institutions in the United States. The research institution partners are Zucrow Laboratories at Purdue University, Air Force Research Laboratory (AFRL) [37], Air Force Institute of Technology (AFIT) [11], University of Central Florida (UCF) [38], and the University of Washington (UW) [39]. This engine has a series of detailed publications outlining performance, operating parameters, and design information [39]. These research programs are sharing the engine in order to increase consistency and comparability between functional RDE experimental data [37].

The project at hand requires a form of validation, and while internal validation between analytical and numerical computation is acceptable in research, it was felt that a more meaningful validation should occur. It should be noted, a numerical simulation was deemed outside of the project deliverables for the course, therefore this form of validation may not be possible. In addition, there was no guarantee experimental testing would occur either to allow for design validation internally, though even if it did, external validation was still desired. As such, due to the large amount of data, literature, and collaboration around the American GH2-GO2 RDE, it was decided that this should the external validation/comparison point for this project. This will become relevant in section 5.1 where the project results are discussed.

2.7 Designing Propellant Feed Systems

There are some notable features common between the different feed systems. For the prototypes that decide to ignite their engine with a DDTT, the propellant bottles feed both the engine and DDTT respectively. To regulate the flow from the feed bottles, some type of valve is used. Sonic nozzles are the more common valve type, but some institutions use needle valves, though there will be higher pressure losses in the needle valves. Along with these flow regulation valves, pressure transducers were placed upstream and downstream as a means of verifying the condition in the nozzle, and thus the mass flow rate. Safety wise, and important features common to these systems was a check valve directly upstream from the RDE, which limits any back flow to propagate up the propellant feed lines. Open-closed type valves are also used (and needed) to control when the propellant will be fed into the system. These valves are usually upstream near the feed tanks, and are of a fast actuation variety. Electric, pneumatic, and magnetic are common to see as fast actuating valves. Temperature sensors are also present in the to monitor the condition of the fluid entering the engine. These features and the configurations serve as a starting point for consideration and development of a propellant feed system fro this project.

Good examples of RDE Piping and Instrumentation Diagram (P&ID) are provided by Mundt [39], Russo [29], Zhou [40], Andrus [41], Burke [42], Shank [43], Ma [44], Ishihara [45], Saul [46], Kindracki [47] and Goto [48].

2.8 Ignition of Rotating Detonation Engines

There are several methods used to ignite a RDE, however, the most common, and most reliable ignition method is using a Deflagration-to-Detonation Transition Tube (DDTT) [1]. According to [49], indirect ignition methods, such as using a DDTT requires less energy to ignite RDE. A DDTT is effectively a Pulse Detonation Engine that is usually tangentially mounted on the RDE, and is pulsed to ignite the RDE then stopped [1]. Research groups using DDTT as an ignition method are University of Central Florida [50], University of Washington [39], Air Force Institute of Technology [11], Air Force Research Laboratory [51], [52].

Other engine ignition methods that are used are automotive spark plugs [53], external flame ignition [35], radial vortex chamber [54], breakable diaphragm to promote single direction propagation [55].

2.9 Thrust Measurement

Typically, small scale rocket engines are tested in a research environment, on a thrust stand, or thrust sled. Typical research environments employ a variety of methods for collecting experimental data for measuring pressure, temperature, mass-flow rate, thrust, etc. [56]. Engine testing best practices, typical sensors, data acquisition systems are described for the Air Force Research Laboratory's EC1 test facility in [56].

There are two main divisions of rocket engine testing facilities, atmospheric ventilation, and blow-down facilities. An atmospheric vented facility allows exhaust gasses to freely escape into the atmosphere. Atmospheric exhaust facilities are located at KTH Royal Institute of Technology [57], MIT [58], National Space and Aeronautical Administration, Air Force Research Laboratory. A blow-down facility entraps exhaust gasses in a blow-down tank, therefore testing can be conducted inside. Blow-down facilities are used at Mcgill [59], National Energy Technology Laboratory [60], Warsaw University [47], University of Washington [39].

The simplest thrust stand design is concerned only with measuring the axially generated engine thrust [61], [62]. More complex facilities, interested in thrust vectoring effects of rocket engines are using multi-axis thrust stands [63]. There are two main designs common for multi-axis thrust stand designs, the horizontal sled [64], [65] and the vertical ring design [29], [66], [67]. The two typical designs for multi-degree of freedom thrust stands are shown in Figure 8.

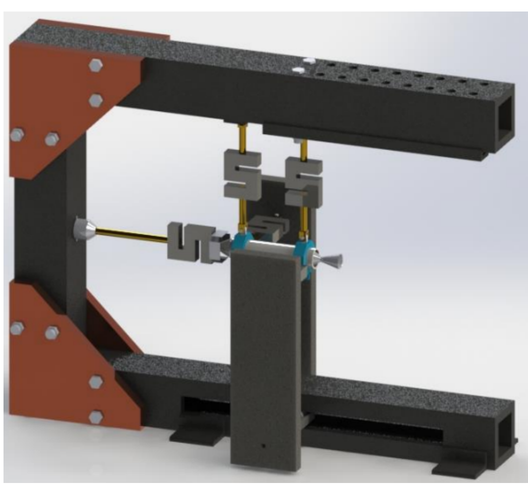

(a) Horizontal Multi-Axis Thrust Measurement [64]

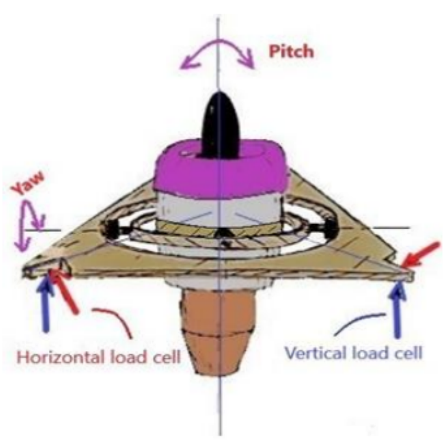

(b) Vertical Multi-Axis Thrust Measurement [66]

Figure 8: Typical Design Concepts for Multi-Axis Thrust Stands

Both orientations have their pros and cons, and are best applicable to different situations depending on the effect that is wished to be studied. Major downfalls of horizontal orientation thrust stands is accounting for gravity effects on friction gliding component, while in the vertical orientation is load cell over-sizing to account for extra mass of frame [63]. In both orientations, the wire-effect must be accounted for, where stiff propellant lines are equipped [63].

2.10 Data Acquisition in Rotating Detonation Engine Testing

Fuel and oxidizer plenum pressures and temperatures are often measured in test RDE's using K-type thermocouples and piezoelectric pressure transducers. Piezoelectric pressure transducers are used because of their high frequencies and ability to measure dynamic pressure fluctuations which makes detecting the rotating detonation wave position possible [68]. Figure 9 from Journell [68] demonstrates this phenomenon where the pressure spikes represent the rotating detonation wave passing over the pressure transducer location. Capillary Tube Average Pressure (CTAP) transducers are also used along the length of the combustion chamber to record an average pressure in the combustion chamber [69]. Recording the transient pressure response in the combustion chamber is difficult and expensive due to the high temperatures in the combustion chamber. When transient response or piezoelectric pressure transducers are flush mounted inside of the combustion chamber they are destroyed by the heat from the combustion process [69].

The RDE being designed for this project is designed to accommodate piezoelectric pressure transducers for measuring the pressures in the fuel and oxidizer plenums as well as one CTAP 12mm away from the combustion front inside of the combustion chamber. The RDE will also be able to accommodate K-type thermocouples for measuring fuel and oxidizer plenum temperatures as well as accommodating thermocouples to be mounted on the exterior surface of the outer body of the RDE. The RDE will be able to accommodate the pressure transducers and thermocouples but procurement and installation of them is out of scope for this capstone project due to their high cost and long lead times.

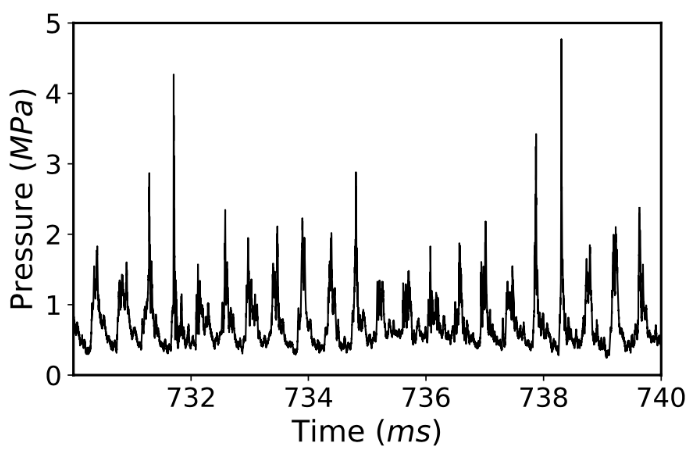

Figure 9: Pressure Spikes Indicating Rotating Detonation Wave Position [68]

Optically observing a rotating detonation wave is a common way to quantify, and characterize different phenomena. In order to record the detonation wave travelling azimuth-ally around the combustion chamber, a mirror can be angled such that a high-speed camera can record the wave propagation, as shown by the basic schematic in Figure 10 [11] [57] [70] [71]. Schelarian imaging can be used to observe the normal component of thrust, expanding within, or beyond he bounds of the engine, as shown in Figure 11 [41].

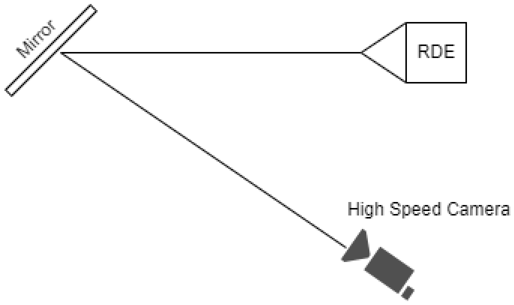

(a) Axial High Speed Imaging Schematic

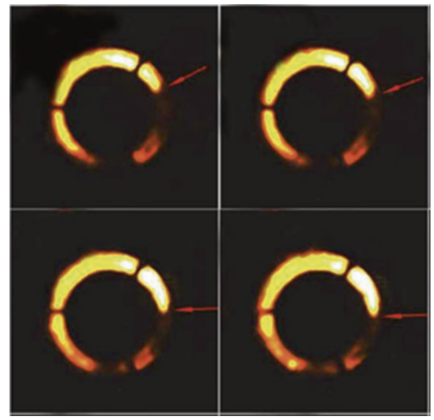

(b) Axial High Speed Imaging Results [71]

Figure 10: Axial High Speed Imaging Schematic and Results

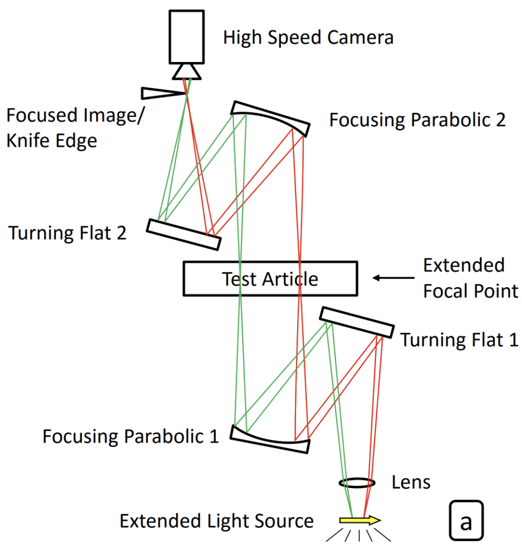

(a) Schlieren Imaging Schematic for Normal Flow Viewing [41]

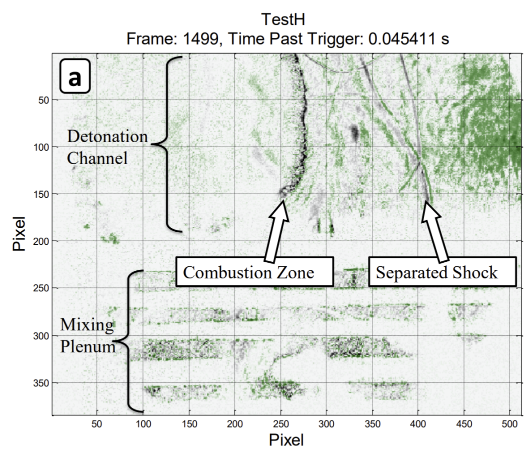

(b) Schlieren Imaging Results of Quarts Outerbody RDE Testing [41]

Figure 11: Normal Schlieren High Speed Imaging Schematic and Results

3 Project Management

3.1 Team Composition

The team took a collaborative approach to complete some project tasks but utilized inter-task cooperation throughout the project for all tasks where dependencies existed. Collaboration also occurred regularly in the form of discussions and brainstorming regarding tasks and sub-tasks. Even where close collaboration occurred on tasks, individuals still held technical ownership of specific sub-tasks such that each member held distinct technical responsibility throughout the project's duration. The following sub-subsections tabulate tasks/sub-tasks owned by each team member.

3.1.1 Shakib Miri

Table 3: Task Summary for Shakib Miri

Task/Sub-Task	Description
Detonation Modelling	Initial portion of the Analytical Model that determines thermochemical properties of a detonation given specific inputs.
Minimum Geometry Calculations	Apply accepted literature correlations to determine minimum engine geometry based on calculated thermochemical properties.
Engine Performance Calculations	Apply accepted equations from literature to determine thrust, propellant mass flow, and specific impulse based on calculated thermochemical properties.
Project Management	Specify tasks and their owner. Create, update, and communicate the project timeline. Schedule and hold internal and external meetings.

3.1.2 Logan Palmer

Table 4: Task Summary for Logan Palmer

Task/Sub-Task	Description
Analytical Model Automation	Expanded the analytical model to iteratively calculate thermochemical, geometry, and performance parameters for ranges of input parameters.
Analytical Model Data Post Processing	Created scripts that visualize data sets from the automated analytical model in graphical form.
Injector Orifice Calculation	Created a script that will calculate the total effective injection area for fuel and propellant respectively given desired pressures and choked flow. The script also calculates required pressures given desired pressures, injector area, and choking condition.
Converge CFD	Defined initial conditions and solver parameters to run 2D-unwrapped RDE combustion simulations. Remodelled injector geometry to more accurately represent intended injector plate design.
Trust Stand Design	Adapted a style of Multi-Axis Thrust Stand that would accommodate RDE configurations matching or similar to the one designed. Appropriate sensors were selected for thrust and vibration data collection.
Funding Acquisition	Reached out to various private and public sources to secure prototype funding.

3.1.3 Aidan Clark

Table 5: Task Summary for Aidan Clark

Task/Sub-Task	Description
Converge CFD	Defined initial conditions and solver parameters to run 2D-unwrapped RDE combustion simulations.
Static Structural Analysis	Setup and ran 3D numerical simulations and hand calculations of the engine combustion chamber to determine pressure-only based stresses. Setup and ran 3D numerical simulations to determine thermal-only based stresses in the engine combustion chamber.
Injector Flow	Setup and ran a 3D numerical simulation that modelled the non-reactive fluid flow through the engine. Focus was placed at the injector orifices into the combustion chamber.
Numerical Simulation Meshing	Hand-generated the quadrilateral discretization mesh to be used in the FEA numerical simulations.
Modal Analysis	Determine the natural frequencies of the engine assembly, compare frequencies to operation frequency to ensure no resonance, or advise design changes if there is.

3.1.4 Patrick Cleary

Table 6: Task Summary for Patrick Cleary

Task/Sub-Task	Description
Preliminary CAD	Based off of the first version of Analytical model results. Created a visual representation of the engine with arbitrary assembly features to begin the DFMA process.
Detailed CAD	Based off of final parameters from the Analytical Model. Created individual parts and an engine assembly that contains all neccessary major features required for engine operation, sensing, and assembly.
Design For Manufacturing and Assembly	Considered manufacturing methods and limitations to change features to achievable during fabrication. Added minor details to accurately represent features that will be present after the fabrication process.
Manufacturing Drawings	Created a drawing sheet template for DETechnologies. Created drawings to the ASME Y14.5 standard for each engine component with sufficient detail to be used for fabrication.
Sensor Selection	Determined suitable pressure and temperature sensors, along with required DAQs and auxiliary equipment, to measure pressure and temperature data at specific locations around the engine to characterize its performance.

3.2 Budget

The following budget breakdown outlines the incurred and anticipated costs for project completion and fabrication of the prototype RDE (Table 7). The anticipated costs are stock material and outsourced machining services.

Table 7: Budget Summary

Description	Cost
ClickUp project management software	$300.00
Metal Pros - Stock Metal	$1,495.00
Outsourced Machining Services	$9,000.00
Team Clothing	$500.00
Total	**$11,295.00**

The material estimate is based on a preliminary quote for a 6" x 1' 316L stainless steel round bar from Metal Pros, using their online quoting tool. The outsourced machining estimate is based on a quote received from Design Manufacturing Inc. (DMI) in Mount Pearl, Newfoundland, for only the base-plate component, costing $3,250.00. This initial quote was extended to the rest of the engine components assuming the injector plate is the same, the outer-body is half the price, and the center-body is 25% of the price; due to the complexity of the parts and tolerances required.

$$Est.Cost = 3250 * 2 + \frac{1}{2}3250 + \frac{1}{4}3250$$

This logic yields an estimated cost of $8,937.50. For budget estimation purposes, this can be rounded to $9,000.00 as shown in the budget summary.

3.3 Meeting Schedule

The Detonation Engine Technologies team meets twice per week for communal working sections, in addition to a time slot reserved for 'as-needed' meetings/working sessions. Supervisor update meetings are bi-weekly, so allow for sufficient progress to be made between meetings, ensuring the most efficient use of people's time. The meeting schedule is outlined in Table 8.

Table 8: Regularly Scheduled Meetings.

Meeting Description	Occurrence
Dr. Duan Update Meeting	Bi-weekly: Wednesdays at 12 (noon)
Group Working Session	Weekly: Mondays from 2pm-5pm
End of Week Update Meeting	Weekly: Fridays from 3pm-4pm
As-needed working session	As-needed: Wednesday 1pm-5pm

3.4 Gantt Chart Timeline

Between the initial planned timeline for the project during this four-month term and the resultant timeline, all major tasks and objectives were achieved, though the order and duration of tasks saw much change. This final project state is presented in the Gantt chart of Fig. 12.

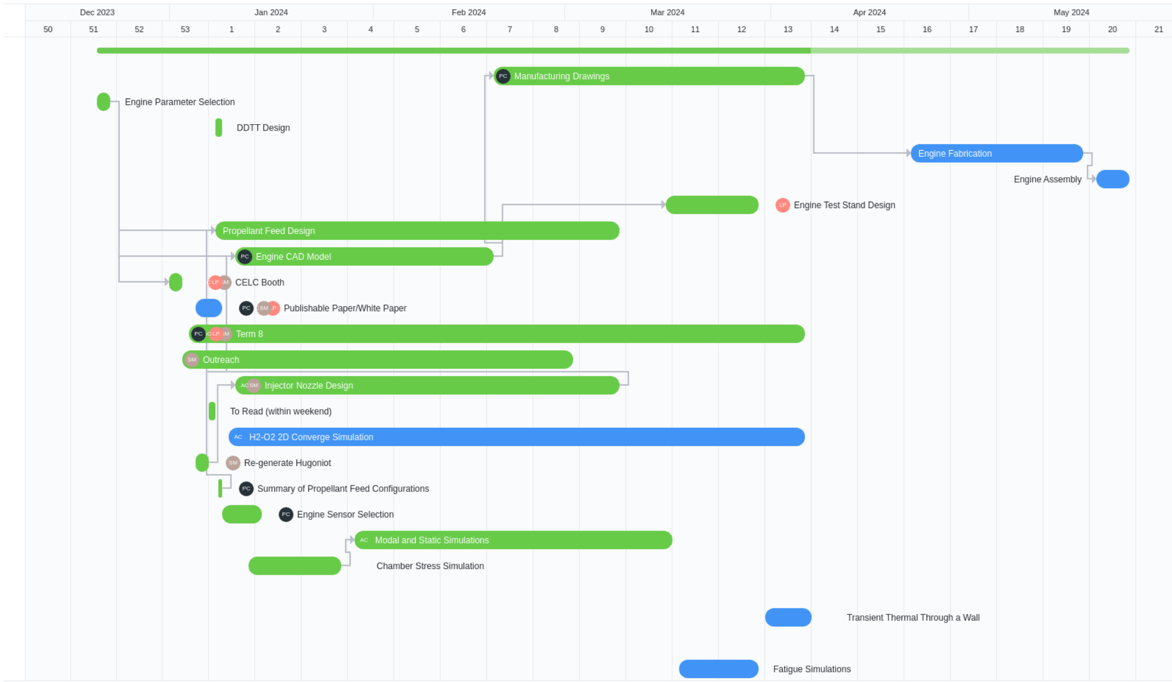

Figure 12: Academic Term 8 Gantt chart with all tasks (in and out of scope), final task durations, and completion statuses

4 Methodology and Results

4.1 Main Engine Design

A number of preliminary qualitative constraints are applied to the engine design to guide the engine design process towards building a safe, reliable and re-usable engine. A summary of qualitative constraints guiding the engine design process are shown in Table 9, according to the syntax -:minimize, and +:maximize. Ballpark quantitative objectives are also shown to gauge approximately the desired solution.

Table 9: Driving Constraints

Parameter	Qualitative Objective	Quantitative Objective
Stagnation Pressure, P_0	-	~ 100 kPa
Stagnation Temperature, T_0	-	~ 18 C
Mass Flow-rate, $\dot{m}$	-	One canister of propellant
Thrust Output	+	1350 N
Engine Outer Diameter, D	+	~ 100 mm

4.1.1 Analytical Modelling

To create initial designs and to obtain a theoretical design point for operation, a set of scripts were developed in MatLab using first-principles formulations from literature and toolbox plugins. Four main calculation functionalities have been developed; detonation modelling, geometry sizing, injector sizing, and engine performance calculation. In addition, two post-processing functionalities were developed, one for results debugging, and one for data analysis and presentation.

4.1.1.1 Detonation Modelling

The detonation model scripting is built from functionalities within the Cantera toolbox [72] and the SDToolbox toolbox [73] [74]. Cantera is an open-source software library for evaluating problems involving chemical kinetics, thermodynamics, and transport processes [72]. Originally developed by Prof. David Goodwin of CalTech, it is now maintained by its community base of users. SDToolbox is another open-source software (Matlab or Python) library that builds off of Cantera to be used to used to solve standard problems of gas-phase explosions using realistic thermochemistry and detailed chemical kinetics [74].

Two of the most important functions contained within SDToolbox are "CJSpeed", "PostShock-eq", and "PostShock-fr". All three of these functions, and the analytical model in general, require a mixture, initial pressure, temperature and appropriate reaction mechanism solver to be defined. "CJSpeed" will determine the detonation wave speed as per the iterative CJ process and theory, given the predefined inputs. "PostShock-eq"takes the predefined inputs and calculated CJ speed to determine the downstream gas properties through a reactive wave, which is analogous to burnt combustion products downstream of the combustion wave within the detonation wave. "PostShock-fr"is very similar to "PostShock-eq" except that is calculates downstream gas properties through a non-reactive wave, like a shockwave, analogous to the leading shockwave in a detonation wave.

The downstream properties from the leading shockwave is the gas state of the induction zone. As described in 2.2, the pressure in the induction zone is the system's maxima, denoted the von Neumann. For design and operation purposes, this parameters is critical to know, hence the need for its calculation.

The downstream properties from the combustion wave are the products that will see expansion and ejection out of the engine to produce thrust. Therefore for later performance calculations, the parameters in this gas state will need to be known. It should be noted that these post combustion state parameters align with the CJ theory conditions. As such, the most important parameter to yield from this state calculation for design and operation, is the temperature, which is the system's maximum.

The final condition that needs calculation with respect to detonation, are detonation wave-specific conditions as prescribed by the ZND theory. Using the "PostShock-eq", "PostShock-fr", "CJSpeed", a ZND specific function "zndsolve", and a constant volume explosion function "cvsolve", the parameters of induction time, induction length, time and distance to mixture 50%, and detonation cell size estimation can be determined. For subsequent calculations, the detonation cell size estimation is the most important and directly applicable parameter. Three different cell size estimations came pre-built in one of the SDToolbox demonstration files, which seem to be the three most widely accepted and quoted methods at the time of the toolbox's release. A fourth correlation found in literature was also added to the calculator, since it was desired to select the best estimation for the H2-O2 propellant mixture. This comparison was warranted through noting that each method was formulated based on specific sets of data for certain gas mixtures, and may not appropriately apply to all input conditions and all mixtures.

All of the included detonation cell size estimations from SDToolbox and Connolly-Boutin's are plotted against experimental data compiled in the California Institute of Technology (CalTech) Detonation Database, published by J. Shepard and M. Kaneshige [75]. The data and correlations in Figure 13 are taken at an initial temperature of 300K.

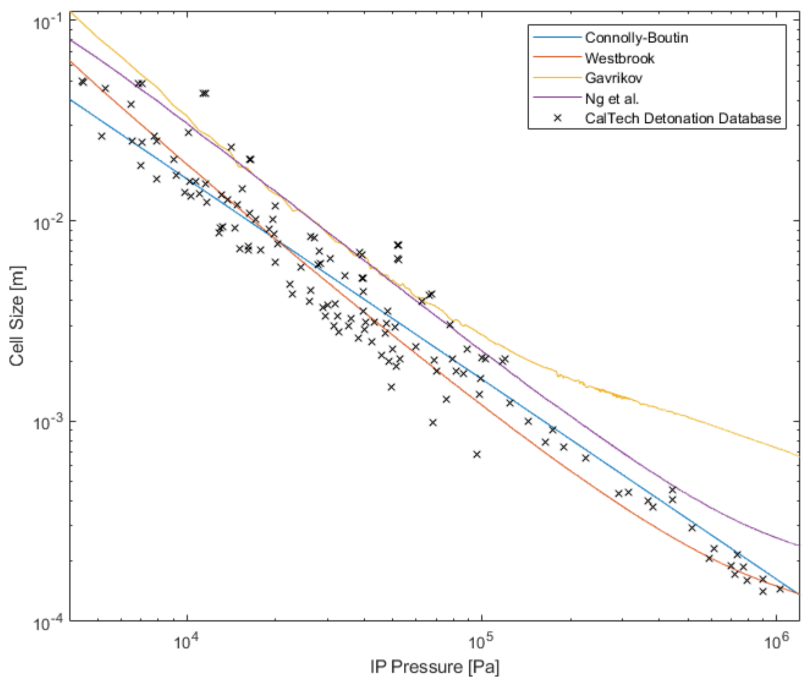

Figure 13: Detonation Cell Size Prediction Comparison to CalTech Detonation Database [75]

All of the estimations show strong correlation to the experimental data, except for the Gavrikov method at high pressures. This discrepancy could be due to an improper implementation of the estimation, as it is challenging to do so.

To determine the dominant factor in the cell size estimations, a nominal value of 130kPa was selected to graph the estimations against a temperature range. Observing the trends and scale in Fig. 14, it is evident that the cell size has negligible variation due to temperature; an approximate change of 0.4mm. The minimal change that is observed is a positive correlation between cell size increase and temperature increase. The particular behaviour observed by the Gavrikov correlation does not currently have an explanation.

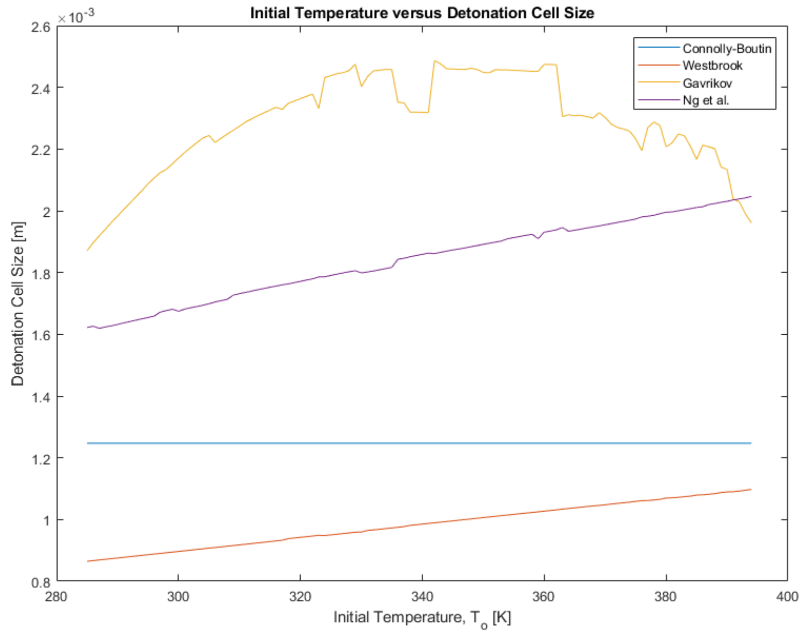

Figure 14: Detonation Cell Size Estimation Behaviour vs Input Temperature

4.1.1.2 Engine Geometry Sizing

According to the predicted detonation parameters as discussed in Section 4.1.1.1, RDE geometry can be deduced. The detonation cell size estimates can be used in conjunction with the combustion chamber geometry rules of thumb, as presented in Table 2 to establish the lower bound of engine feasibility. Bykovskii's combustion chamber geometry rules of thumb are multiples of the detonation cell size parameter only, therefore, plotting the geometry as a function of initial pressure and temperature will follow a similar curve shape to that shown in Figure 13 [28]. The deviation in detonation cell size predictions creates a range of minimum geometry for each combustion chamber geometry. Combustion chamber geometry parameter labels are depicted by the RDE schematic in Figure 15.

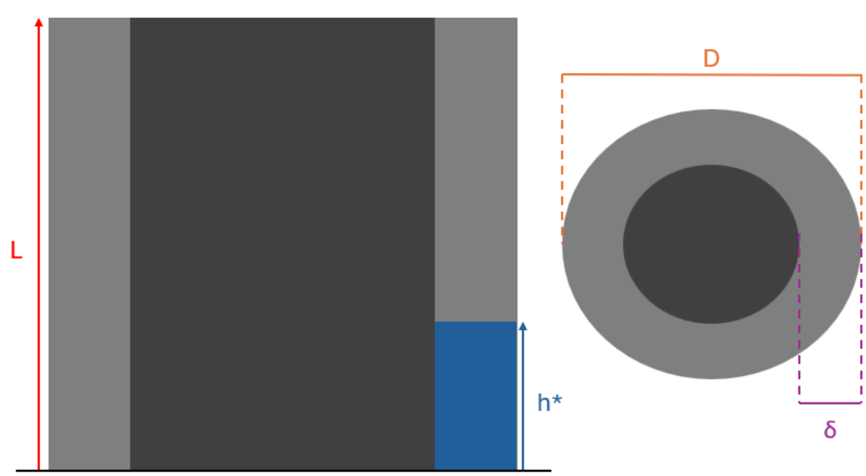

Figure 15: Engine Combustion Chamber Geometry

The upper and lower prediction bounds for the four primary combustion chamber geometry are depicted by the dotted and solid lines in Figure 16

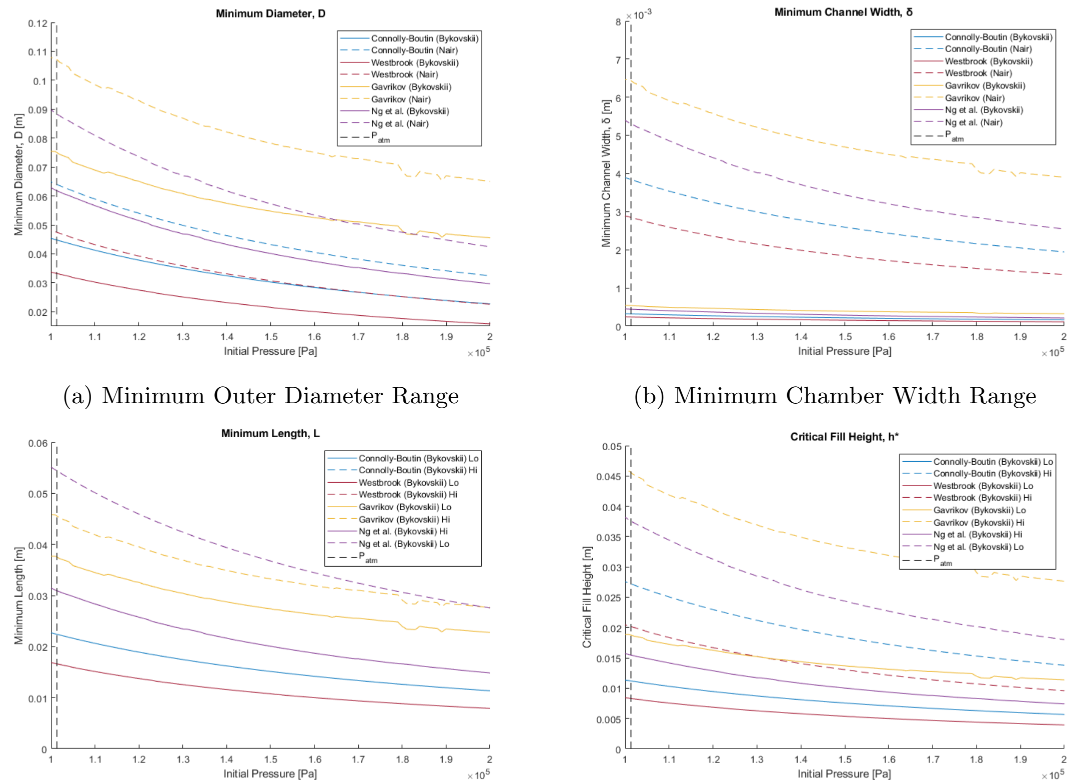

(a) Minimum Outer Diameter Range

(b) Minimum Chamber Width Range

(c) Minimum Chamber Length Range

(d) Minimum Fill Height Range

Figure 16: Minimum Ranges of Combustion Chamber Geometry

The above presented results are minima geometry associated with sufficiently constricting the combustion wave such that it is accelerated to the supersonic regime. For simplicity of further discussion, the cell size correlation presented by S. Connolly-Boutin [36], will be used because it has the best agreement with the experimental detonation results presented in the CalTech detonation database [75]. The critical fill height parameter range adjustment factor of 12 ± 5 will be simplified to a nominal value of 12, for the sake of discussion.

The mass flow rate, is determined by considering the amount of propellant that is required to replenish the critical fill volume of propellant between subsequent waves. For n number of concurrent combustion waves, the mass flow rate can be determined as shown by Equation 8.

$$\dot{m} = \frac{V_p \rho}{t} \tag{8}$$

Where ρ is the combined mass averaged density of the propellant mixture, t is time between subsequent combustion waves, broken down by Equation , and V_p is the volume of fresh propellant, broken down in Equation 10.

$$t = \frac{C_{av}}{nV_{CJ}} \tag{9}$$

Where V_{CJ} is the detonation wave velocity, n is the number of concurrent detonation waves, and C_{av} is average circumference of the combustion chamber. The volume of fresh propellant is shown by:

$$V_p = \delta h^* C_{av} \tag{10}$$

Combining Equations 8, 9 and 10 Equation 11 is obtained.

$$\dot{m} = nh^* \delta \rho V_{CJ} \tag{11}$$

With a relation for mass flow rate established, the thrust generated from an RDE of known geometry can be calculated, according to the specific thrust equation from by Shepherd in Equation 7 [31]. The thrust curve, detonation cell size prediction for increasing initial pressure is shown in Figure 17.

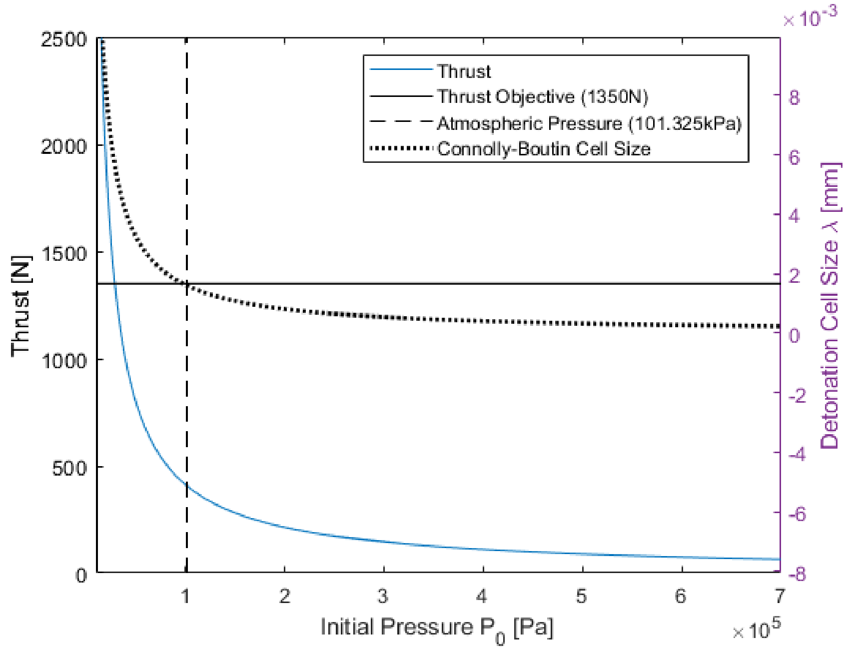

Figure 17: Thrust Curve

As shown by Figure 17, the thrust created by the minimum engine geometry required to reach detonation combustion, as per Bykovskii's rules [33] is very low at initial pressures above atmospheric.

In order to size an engine to reach the thrust target of 1350N, more propellant must be added to the combustion chamber, thereby increasing the propellant critical fill height beyond the minimum.

From the selected minimum engine geometry, the resultant thrust according to the minimum critical fill height, and thereby mass flow rate, is 322N. Rearranging Equation 7 to solve for mass flow rate, at a thrust target of 1350N, finds a required mass flow rate, in single wave mode, of 334.72 $\frac{g}{s}$. From the selected combustion chamber geometry, the critical fill height to hit the thrust target of 1350N is calculated by rearranging Equation 11 for h^*, finding a fill height of 37.53 mm. This method also shows, that dual wave mode would not be able to reach the thrust target, as the required mass fill height would exceed the combustion chamber length.

4.1.1.3 Summary of Results

Selected parameters defining the combustion process, propellant feed, and combustion chamber geometry, as previously presented are summarized in Tables 10 and 11.

Table 10: Summary of Select Final Combustion Parameters

Parameter	Value
Detonation Cell Size, λ	1.214707 mm
Initial Temperature, T_0	300 K
Initial Pressure, P_0	130 kPa
Equivalence Ratio, ϕ	1.00
Mass Flow Rate, $\dot{m}$	334.72 $\frac{g}{s}$
Specific Impulse, I_{SP}	410.6716 s
Peak Pressure, P_{VN}	4299196.4247 Pa
Peak Temperature, T_{CJ}	3720.2403 K
Combustion Speed, V_{CJ}	2848.5565 $\frac{m}{s}$

Table 11: Summary of Final Engine Geometry

Parameter	Value
Thrust Goal	1350 N
Fill Height, h^*	37.52731 mm
Chamber Outer Diameter, D	60.00 mm
Chamber Inner Diameter, D	50.00 mm
Channel Width, δ	5.00 mm
Length, L	50.00 mm

4.1.2 Finite Element Analysis

The Finite Element Analysis of this project is entirely conducted in Altair HyperMesh, using the OptiStruct solver. The engine mesh is created semi-manually so that the element quality accurately reflects the true engine geometric features and does not add artificial model stiffness. This results in a mesh that is primarily formed from first-order hexahedral elements, with minimal amounts of first-order pentahedral elements.

4.1.2.1 Model Setup

The finite element model of the engine, uses a linear, isotropic material model, with materials defined as per Table 12.

Property	Value	Units
Density	8.00	g/cc
Tensile Strength (Ultimate)	550	MPa
Tensile Strength (Yield)	240	MPa
Elongation at Break	60%	
Modulus of Elasticity	193	GPa
Poisson's Ratio	0.298	

Table 12: Mechanical Properties of 316 Stainless [76][77]

The mesh used in the finite element model uses primarily first-order hexahedral elements. Hexahedral mesh was chosen because the engine is primarily cylindrical, which allows a fairly simple meshing process, without the need for implementing computationally expensive second-order tetrahedral elements.

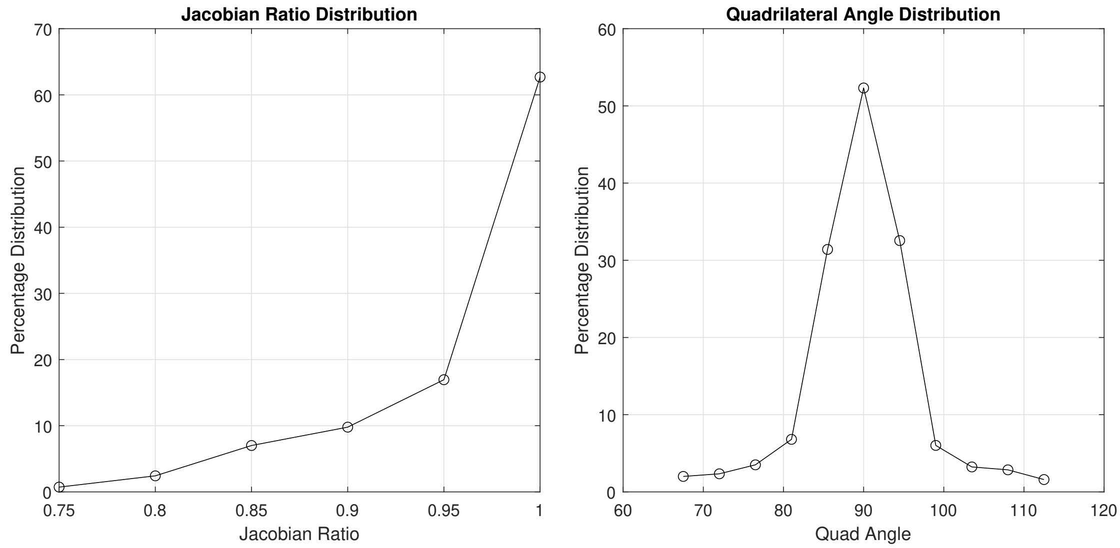

Figure 18: Critical 3D Mesh Metrics

The above, Figure 18, demonstrates that the 3D mesh used for all FEA is of high quality. Specifically, the charts show the distribution of Jacobian ratio and quadrilateral angle for all 3D elements in the mesh.

$$[J]_{3D} = \begin{bmatrix} \frac{\partial x}{\partial \xi} & \frac{\partial y}{\partial \xi} & \frac{\partial z}{\partial \xi} \\ \frac{\partial x}{\partial \eta} & \frac{\partial y}{\partial \eta} & \frac{\partial z}{\partial \eta} \\ \frac{\partial x}{\partial \zeta} & \frac{\partial y}{\partial \zeta} & \frac{\partial z}{\partial \zeta} \end{bmatrix} \tag{12}$$

First off, it is important to understand what a Jacobian ratio is, and what this metric can show with regards to mesh quality. The Jacobian matrix, shown in Equation 12, provides information about the volume, shape and orientation of each element in a mesh [78]. More specifically, the Jacobian ratio is the ratio between smallest and largest values of the determinant of the Jacobian matrix - and in this case, which is calculated at the nodal points [79]. A Jacobian ratio of 1 means that the element is perfect.

4.1.2.2 Bolt Pre-loading

Bolt pre-loading calculations for analysis and sealing, were conducted using M5 bolt size, at SS 12.9 grade. Fastener loading conditions are calculated based on the following, Table 13:

Table 13: Fastener Loading Conditions

Load	Value
Chamber Pressure	35 MPa
Area of Applied Pressure	864 mm^2
Number of Bolts	12
Total Load	30.24 kN
Load per Bolt	2.52 kN

WIthin the FEA model, these fasteners were modelled in 1D with the use of RBE and BEAM elements. The 1D bolt idealization is shown below, in Figure 19. Once these bolts were modelled a the preload was applied to each fastener, allowing for accurate modelling of the sealing used - and the resulting stresses caused by the bolt torque.

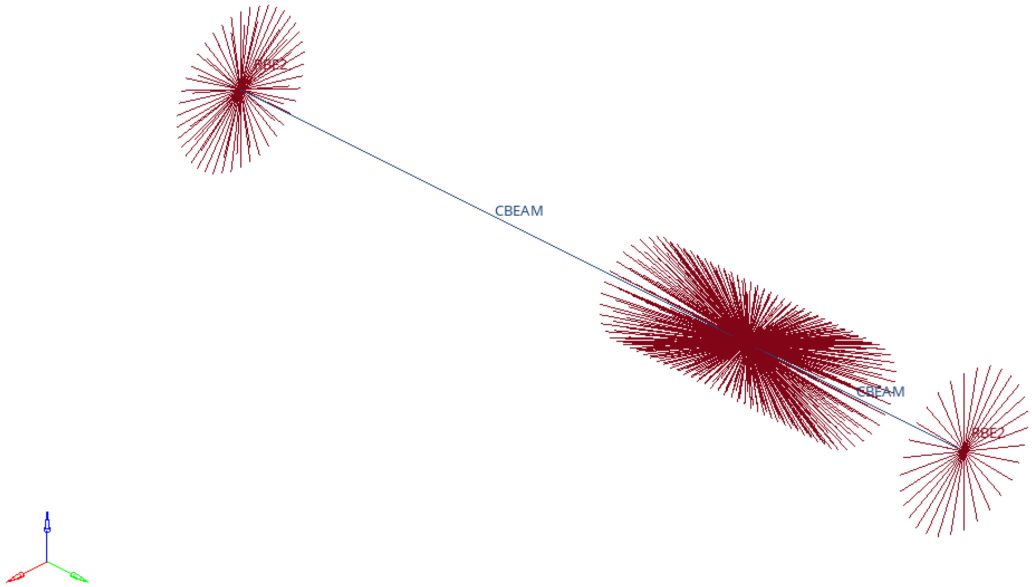

Figure 19: 1-D FEA bolt idealization

This image, Figure 19, shows the RBE in red, with the BEAM elements shown in blue. It is important to note that the BEAM elements use a cross-section property to accurately represent the diameter of the fastener, and use material properties to match that of the selected bolt grade.

4.1.2.3 Modal Analysis

For this project, where the rotating pressure wave rotates at high speed and frequency - it is important to consider fundamentals of rotor dynamics. For this preliminary analysis, the natural frequencies of the structure were examined to ensure that none of these frequencies fall near the steady state operating frequency of 16,493.7 Hz.

Table 14: First 6 Modes of the RDE

Mode	Frequency (Hz)
1	185.63
2	295.16
3	295.16
4	403.00
5	874.69
6	874.70

Table 14 shows the first six natural frequencies, and it is clear that none of these fall within 15% of the operating frequency. Further rotordynamic analysis would prove useful, as it would allow a better understanding of how the engine will behave near natural frequencies.

Extending the analysis to operating frequency, which is determined to be 16,493.661 Hz, will allow an understanding of if resoance is a problem in the engine.

Mode	Frequency (Hz)
39	15,949.40
40	16,488.80
41	16,586.99

Table 15: Modes near operating frequency

Per Table 15, Mode 40 is within 5 Hz of the operating frequency - which is of concern for the operational life of the engine. This discovery came late in the design process, and prior to moving to manufacturing, the team will further investigate this concern to ensure the engine does not operate at a resonance frequency.

4.1.2.4 Static Loading

Two static scenarios were analyzed as part of the preliminary structural analysis. These two scenarios include peak pressure and peak temperature due to H_2-O_2 detonation as discussed in the analytical model. Load conditions are described below in Table 16:

Table 16: Load Conditions

Load	Value
Pressure	4.2992 MPa
Temperature	3720.2403 K

Pressure is applied to the inner wall of the outer body, as well as the center body, and applied normally to the inner face of each element.

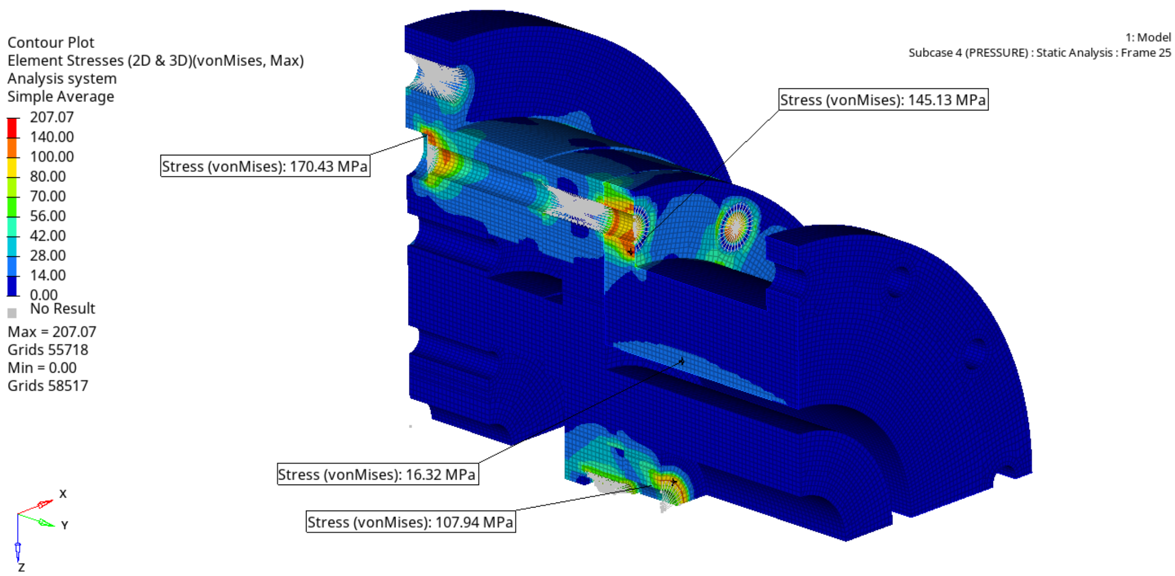

Figure 20: Contour Plot of Stress due to Static Pressure Loading

As per Figure 20, there are several high-stress locations, most of which are located near the fasteners - which is expected. Due to the preload required for sealing, and the design of the combustion chamber, it is expected that the fastners and surrounding areas will experience most of the stresses. A particular area of concern early on in design was the combustion chamber walls, where a maximum stress under only pressure loading is 16.32 MPa - well below the material yield strength.

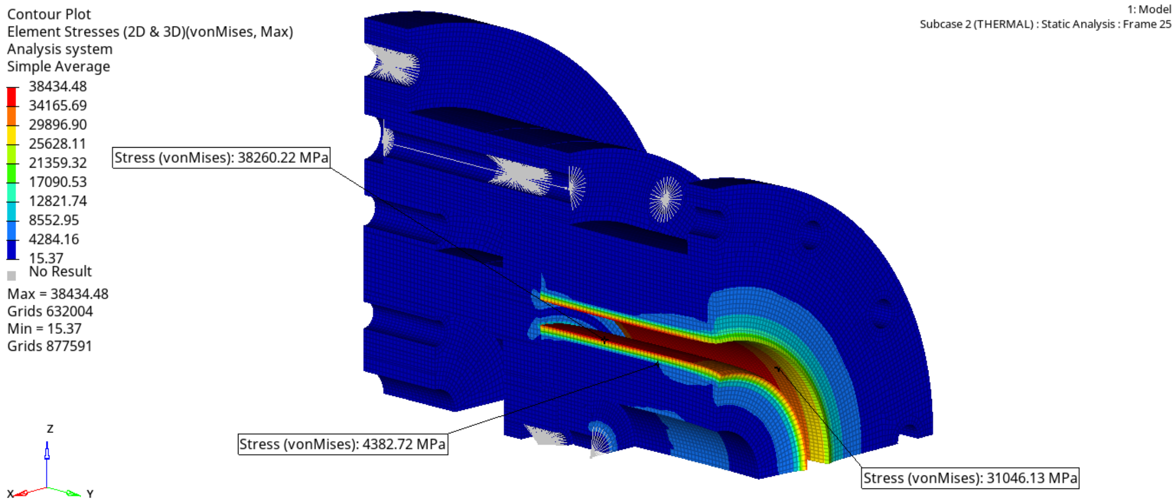

Figure 21: Contour Plot of Stress due to Static Temperature Loading

The above, Figure 21, is a static loading scenario of the inner walls of the combustion chamber under a maximum detonation temperature of 3720 K as determined by the analytical model. Due to time constraints, a transient model was not able to be fully analyzed, and as such this model does not accurately represent stresses caused by this temperature.

4.1.3 Computational Fluid Dynamics

4.1.3.1 Combustion Modelling

The combustion process is modelled using Convergent Science's ConvergeCFD software [80]. A 2D, unrolled, Hydrogen-Air RDE is provided through partnership with the Convergent Science team, as a starting point for model development. Modifications and current progress to converting the 2D unrolled RDE model from Hydrogen/Air combustion to Hydrogen/Oxygen is described below. 2D RDE geometry is shown in the ConvergeCFD interface in Figure 22.

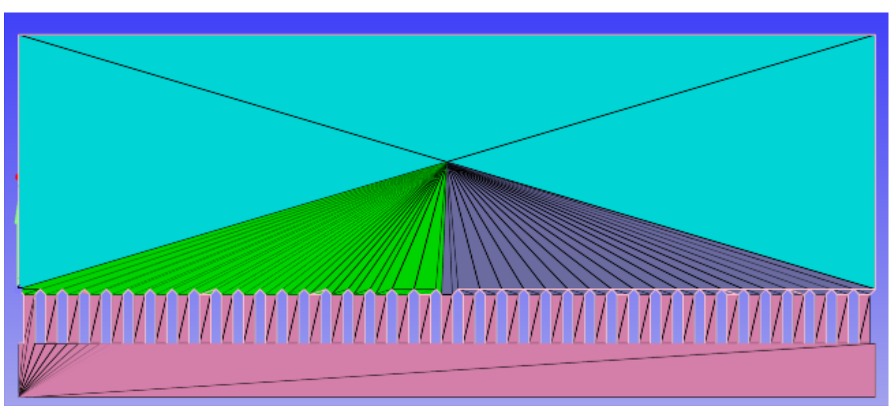

Figure 22: ConvergeCFD 2D RDE

The geometry for this RDE is shown by the drawing in Figure 23.

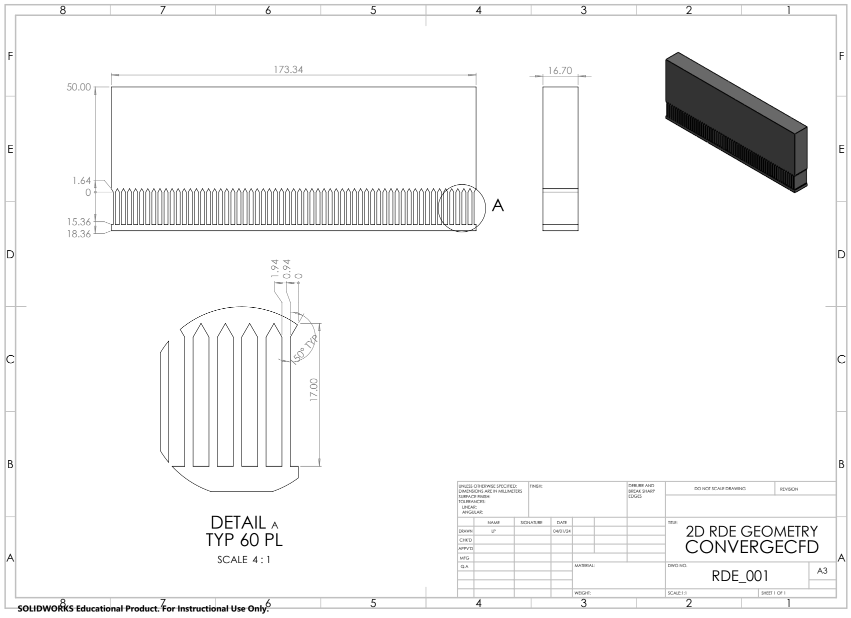

Figure 23: 2D RDE Geometry

The geometry shown in Figure 23 is chosen to replicate the 3D RDE. The length of the 2D engine is the circumference of the centre of the combustion chamber of the 3D engine. The height of the 2D engine is identical to that of the 3D engine. Injectors are sized in order to choke the flow at a mass flow rate of 335g/s, according to the same pressure differential in the 3D engine.

Initiation of the 2D RDE requires a hot, high-pressure ignition zone, and cold, low-pressure pre-ignition zone to initiate a rotating wave. The hot ignition zone is shown by the purple triangle on the right-hand side of Figure 22. Figure 24 shows the first few steps of an RDE ignition. It is important to recognize that the hot, higher-pressure ignition zone is on the left-hand side, shown by the red triangle; opposite of the previous discussion.

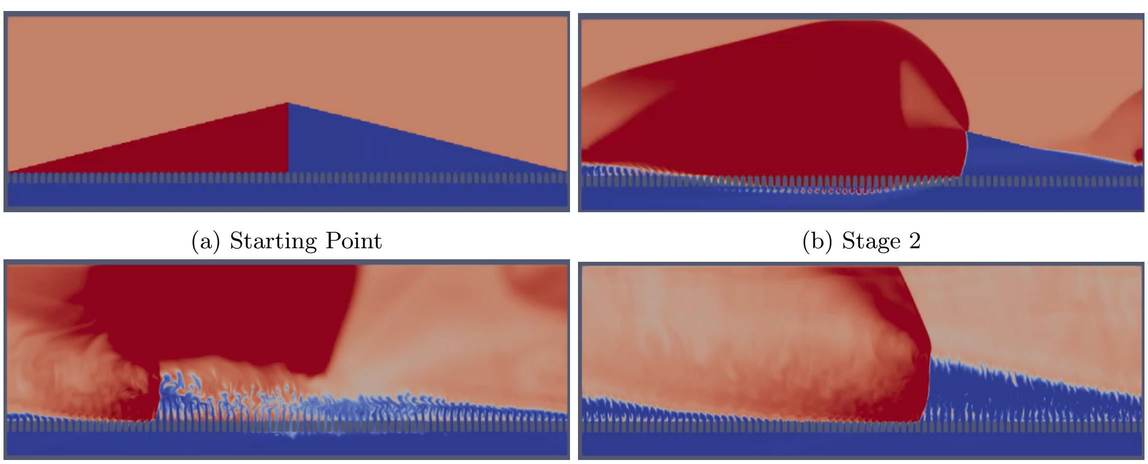

(a) Starting Point

(b) Stage 2

(c) Stage 3

(d) Steady State

Figure 24: RDE Combustion CFD Initiation [80]

Figure 24 shows a Hydrogen and Nitrogen diluted Oxygen simulation of the combustion process within an RDE. As seen, the coupled ignition/pre-ignition zones induces a pushing-sucking behaviour to 'pull' the combustion wave to the right side. After the starting point, no further artificial behaviours are applied to the simulation. It is seen that the combustion wave begins to die out, in stage 3, before growing into the steady-state detonation wave shown.

Current results for stoichiometric Hydrogen and Oxygen combustion CFD model are promising, but have not been finished within the time constraints.

4.1.4 Design For Manufacturing and Assembly

Figure 25 outlines the parts in the engine assembly and Table 17 has their respective names. The engine is made up of 4 parts, the base plate, injector plate, outer body, and centre body. The base plate acts as the main mounting point of the assembly and accommodates the fuel and oxidizer inlets and the pressure transducers.

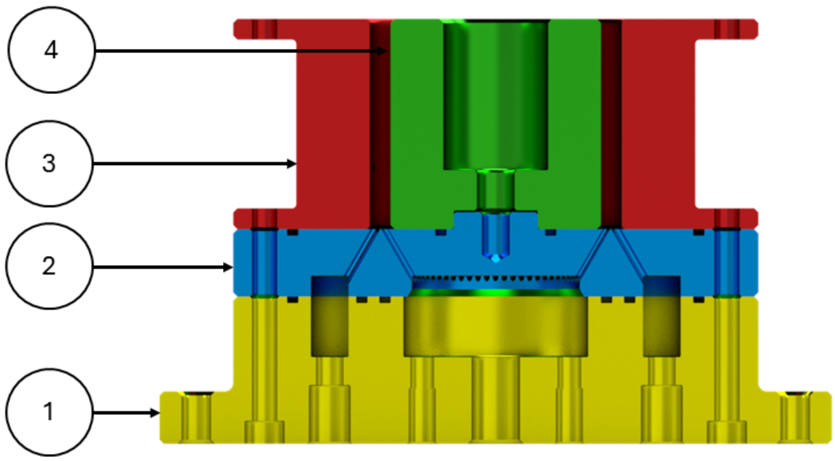

Figure 25: Engine Assembly

Table 17: Figure 25 Engine Parts

Part No.	Part Name
1	Base Plate
2	Injector Plate
3	Outer Body
4	Centre Body

4.1.4.1 Chamber Alignment

The alignment between the centre body and the outer body bore is critical for a concentric annular combustion chamber. M6 precision ground dowels are used as locating features. The dowels are used between each part interface such that a new reference surface is established and the tolerance stack is not carried from the base plate to the annular chamber. The dowels are installed in the plates with an H7/p6 interference fit [81] for a maximum and minimum interference fit of 20 and 0 microns. The other ends of the dowels slide into H7/h6 precision sliding fit holes with a maximum clearance of 20 microns. [81]. The feature labelled datum B in Figure 26 on the injector plate is used to align the centre body and the shaft/hole fit between the two is also an H7/h6 precision sliding fit with a maximum clearance of 37 microns. The positional tolerance on the bore of the outer body is 50 microns and the allowed runout between the alignment feature bore and outer diameter of the centre body is 10 microns. This stack-up results in a maximum of 117 microns of misalignment between the centre body OD and outer body bore. These tolerances and misalignments are optimized for manufacturing cost and engine performance.

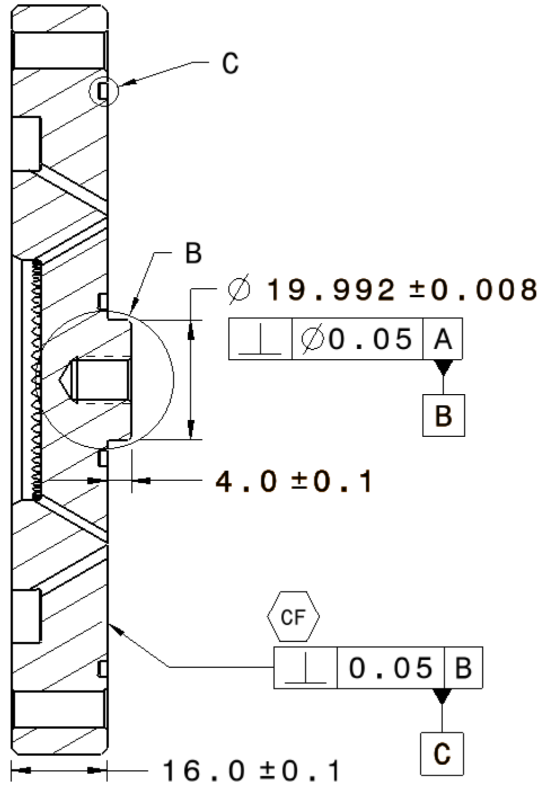

Figure 26: Centre Body Locating Feature

4.1.4.2 O-Ring Sealing

The engine relies on axial O-Ring sealing to seal the fuel and oxidizer plenums to prevent mixing before the combustion chamber and to seal the combustion chamber from exhaust gases escaping between the stacked plates. The O-Ring features can be seen in Figure 25 as the rectangular features on each plate seam. The O-Rings are nitrile rubber and are compatible with oxygen and hydrogen. The O-Ring features and finishes as shown in Figure 27 were sized using the Trelleborg Solutions O-Ring calculator [82] to ensure the proper compression, housing fill and stretch.

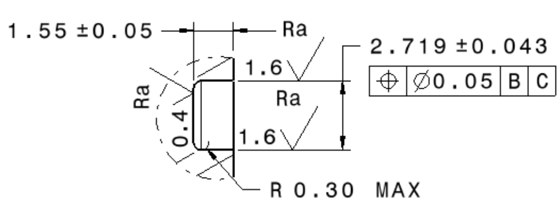

Figure 27: O-Ring Feature Detail

4.1.4.3 Manufacturing Considerations

Precision manufacturing and holding tight tolerances is common with parts in rocketry. Some manufacturing procedures will be specified to the manufacturer. The most pertinent one will be to machine the bore of the annular combustion chamber after the engine has been assembled with dowels and bolted together. This will ensure that there is minimal runout between the centre body outer diameter and outer body inner diameter becasue both features are machined in the same operation. Another crucial procedure for manufacturing is measuring the machined parts. The datum strategy established in the drawings package require the parts be measured in a specific way with reference to the respective datums. These measurements are often taken with a Coordinate-Measuring Machine (CMM). A CMM machine can measure the respective features correctly with respect to their specified datum and record the measurement and document it with the respective callout. These are documented in a dimensional report that is sent back to the part designer so the designer will know if the tolerances have been met. These dimensional reports will be requested and required for DETechnologies's parts so the team knows if the tolerances have been met and the team can revisit the tolerance stacks. This allows the team and designer to know what they are actually working with in terms of the dimensions of the features on the parts.

4.2 Injector Plate Design

4.2.1 Analytical Modelling

The injector plate must be designed such that the propellant feed is choked at the desired mass flow rate. This will ensure no back-propagation of combustion bi-products, or actively combusting propellant. A conservative, mass choking approach is taken, considering a control volume between propellant plenums across the injector plate, into the combustion chamber, shown in Figure 28.

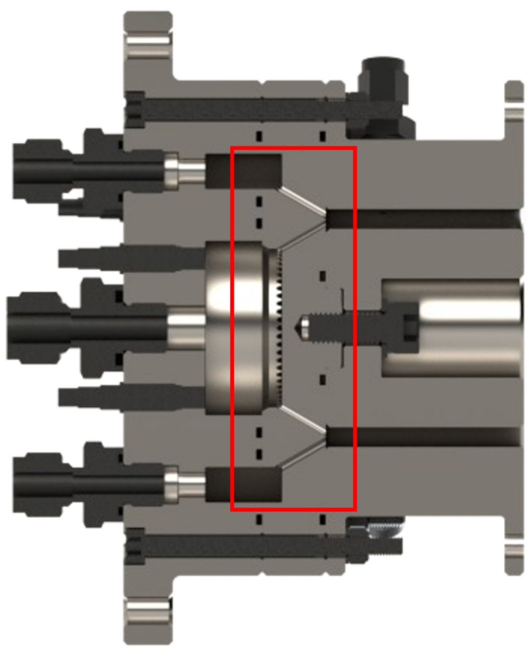

Figure 28: Injector Plate Control Volume

From the conservation of mass across a control surface, the mass flow rate is shown as Equation 13 [83].

$$\dot{m} = \frac{P_o}{\sqrt{RT_o}} A \sqrt{\gamma} M \left(1 + \frac{\gamma - 1}{2} M^2\right)^{-\frac{\gamma+1}{2(\gamma-1)}} \tag{13}$$

Where M is mach number, P_o is stagnation pressure in the plenum, R is the gas constant, T_o is the stagnation temperature in the plenum, γ is the specific heat ratio. Choked flow is defined by a Mach number of 1, setting M = 1 and rearranging for stagnation pressure, we reach Equation 14 [83].

$$P_o = \dot{m} A \sqrt{\frac{\gamma}{RT_o}} \left(1 + \frac{\gamma - 1}{2}\right)^{-\frac{\gamma+1}{2(\gamma-1)}} \tag{14}$$

In order to size the injector plate, Equation 14 is applied to iterative calculate the stagnation pressure, across a range of injection areas. The ratio of injection area to surface area of the annular combustion chamber is defined as the Area Ratio.

$$AreaRatio = \frac{A_i}{A_a} \tag{15}$$

With all parameters in Equation 14 known, the area ratio is varied across the possible realm from 0:1 in order to minimize the upstream plenum pressure. A physical feasibility constraint is applied to the area ratio, limiting the upper threshold to be < 0.25. A feasibility constraint to the upstream pressure is also applied, to ensure sufficient pressure differential across the control surface to reach choked flow condition. The pressure differential constraint is defined by John [83] as

$$P_o > 1.89P_d \tag{16}$$

Where P_o is upstream, stagnation pressure, and P_d is the downstream pressure. From here, the minimum stagnation pressure can be calculated, recalling the downstream pressure objective.

$$P_o > 1.89 * 130kPa > 245.7kPa \tag{17}$$

In order to satisfy both area ratio and plenum pressure constraints, the plenum pressure is increased to three times the minimum, such that the area ratio constraint is satisfied. The raw iterative process to narrow in on an area ratio for both Hydrogen and Oxygen injectors is presented in Appendix C.4.

Results of applying the above described approach is summarized in Table 18.

Table 18: Preliminary Injector Parameters

Param	**Oxygen**	**Hydrogen**
Plenum Pressure	737.25 kPa	737.25 kPa
Area Ratio	0.1880	0.0944
Area [m^2]	162.42e-6	81.55e-6

It is important to note that the above starting point has a total injection area ratio of 0.269, so real manufacturing constraints should tend towards lesser injection area where possible. Understanding a feasible starting point to implement choked flow at the injector plate, manufacturing and mixing constraints are applied. Manufacturing constraints define the injection area as N integer number of same diameter straight walled drilled holes of real metric drill size. Mixing constraints imply that the N integer number of injector holes for both Hydrogen and Oxygen are the same, such that the ejected flow stream can be set to intersect.

Applying these constraints to find an realistic injector plate design that resembles the preliminary design varies the final results slightly. The final injector plate design parameters are calculated according to Appendix C.5 and summarized in Table 19.

Table 19: Summary of Injector Plate Parameters

Parameter	**Hydrogen**	**Oxygen**
Plenum Pressure	1102.126352 kPa	975.702558 kPa
Injector Area Ratio	5.4545 %	12.2727 %
Injector Area Specifics	60 x ϕ 1 mm	60 x ϕ 1.5 mm

Since mass flow rate is a parameter that will be varied during experimental testing, a plot of mass flow rate versus stagnation pressure in the supply plenums is shown in Figure 29.

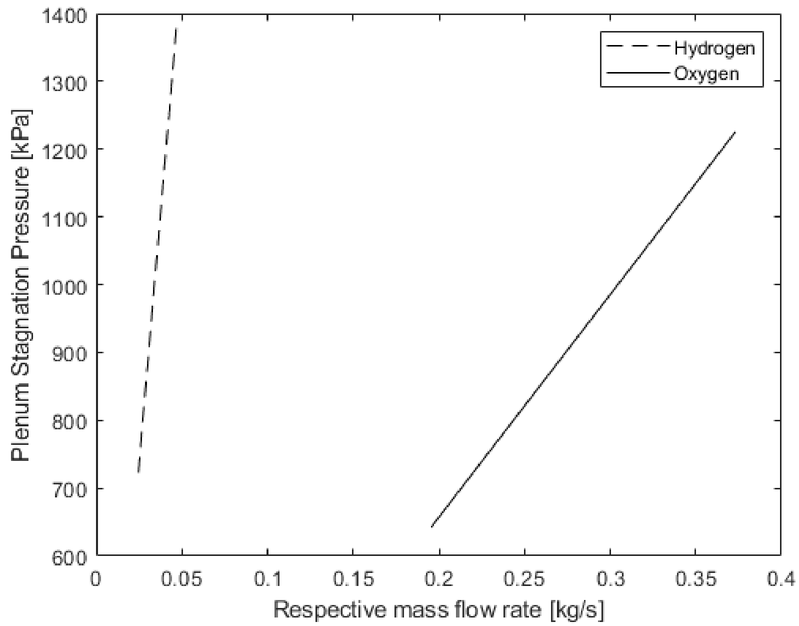

Figure 29: Individual Plenum Pressures to Attain Choked Mass Flow Condition

4.2.2 Numerical Simulation

The injector for both hydrogen and oxygen must choke the propellant flow, and to verify that this will happen, a 3D volume model of the interior of the RDE in Converge CFD [80]. In addition to validating the choked flow condition, this model will serve to analyze mixing in the chamber.

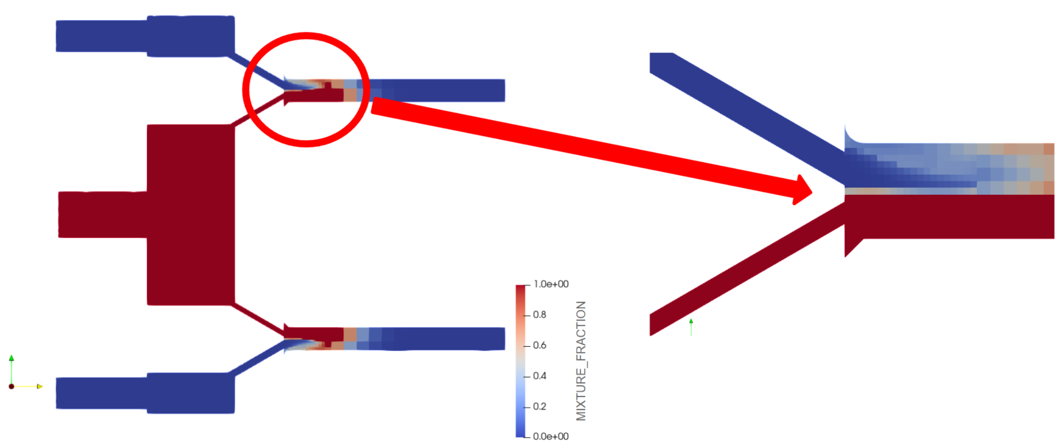

Figure 30: Section view of mixture fraction contour plot in Converge CFD

The above, Figure 30, shows the hydrogen (red) and oxygen (blue) feeding into the combustion chamber. From this image, it is clear that the independent propellant streams do not mix very well - which can be investigated further using a contour plot of the Mach number in this model.

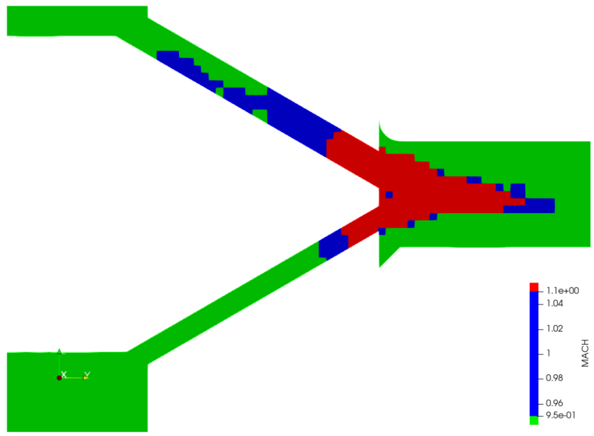

Figure 31: Section view of Mach number contour plot in Converge CFD

Figure 31 shows three distinct phases of Mach number in the injectors and combustion chamber. Red denotes supersonic flow, blue denotes flow at Ma = 1, and green represents subsonic flow. Investigating these results further, the limited mixing at the beginning of the combustion chamber (as seen in Figure 30) is to be expected, because at that point, flow is supersonic, and due to fundamental gas dynamics, flow in supersonic regime does not mix well. Figure 31 also helps validate the choke flow condition required in the injectors, as the flow exiting the injectors is supersonic.

4.3 Propellant Feed System

This design was built as a compilation of existing published literature to quantitatively analyze the compressible fluid flow from propellant storage tanks to the engine, such that a model could be developed that feeds stagnation conditions and mass flow rate, based on a specific feed system, into the analytical model. Inversely, the optimal desired stagnation and mass flow rate for engine performance could be used to back-calculate specific parameters like pipe diameter and length to determine or validate if a feed system will work for an engine design. These functionalities will further refine the analytical model outputs to be more accurate estimations of lab performance. The basis for this P&ID is borrowed from similar engines operating on gaseous fuels that are available publicly, as discussed in Section 2.7

At a high level, the gaseous oxygen and gaseous hydrogen are supplied separately by fuel tanks on site. The propellants flow from the supply tank through a pressure regulator, sonic nozzle, fast actuating valve, and check valve respectively until they reach the respective fuel and oxidizer plenum in the RDE. The fuel and oxidizer lines also branch off from their main lines to supply fuel and oxidizer to the DDTT. The pressure regulator is used in conjunction with the sonic nozzle to choke the fluid flow and control the mass flow rate as supported by Equation 13 from John [83]. Pressure transducers are used directly upstream and downstream of the sonic nozzles to ensure a choked flow condition. Pressure transducers are also used directly inside the propellant plenums to ensure choked flow condition.

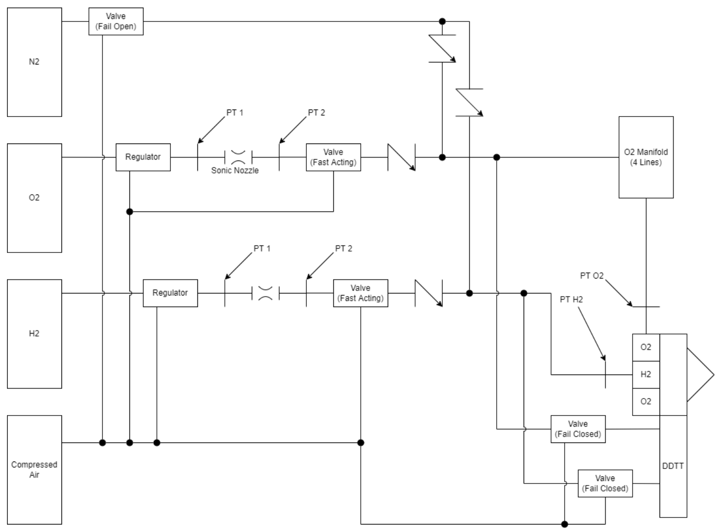

Figure 32: Preliminary Piping and Instrumentation Diagram

Collaborating with Dr. Sean Connolly-Boutin yielded design direction regarding compressed gas cylinders. Due to the very small orifice at the top of standard compressed gas cylinders, the flow rate that is achievable with these tanks is very low, unless many are connected together with a manifold. The method that was developed for Concordia has a large orifice off-the-shelf compressed gas cylinders functioning as the feed tank, with standard gas cylinders teed off the main feed line to be used to fill that feed tank.

4.4 Thrust Stand

In order to reach experimental testing and validation of the RDE design presented in previous sections, a corresponding thrust stand must be designed that is capable of measuring the thrust generated. In the field of small scale rocket engine testing there are two main designs for a thrust stand, as presented in Section 2.9. The major dividing difference is the objective of experimental testing, whether single or multiple Degree of Freedom (DOF) thrust measurements are desired. Given the low Technology Readiness Level of RDE technology, and the introductory level of experimental testing planned; a single DOF thrust stand would be sufficient. However, due to the inherent thrust vectoring effect that RDEs have, it is deemed sufficiently important to lay out the groundwork for building a multi-DOF thrust stand.

With the objective of building a multi-axis thrust stand in mind, conceptual design is borrowed from Russo [29], Rezende [66] and Carpenter [67]. These similar conceptual designs are selected as it eliminates the cantilever effect that gravity induces on the engine. With these conceptual designs in mind, the thrust stand in Figure 33a is designed.

The presented thrust stand is a 3-axis thrust stand, able to measure axial thrust in Z, and thrust vectoring moments around X and Y. The available DOF of the designed stand are shown in Figure 33b.

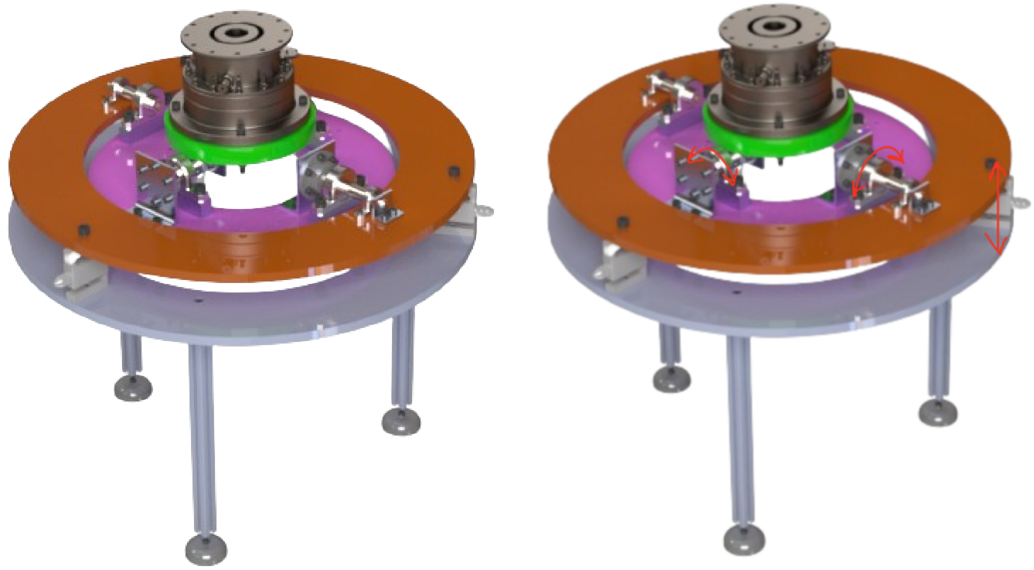

(a) Thrust Stand

(b) Thrust Stand Design DOF

Figure 33: Preliminary Thrust Stand Design

4.4.1 Choosing Load Cells

The inherent thrust vectoring effect that RDEs have is a function of the number of simultaneously rotating combustion waves within the combustion chamber, and the eccentricity of the combustion chamber channel. In single wave combustion mode, one detonation wave traverses around the cylindrical combustion chamber in the azimuth direction, while the oblique shock wave extends axially outwards. The thrust generated can be simplified by considering the axial component of thrust to be a force on the injector plate, at azimuth position θ for time t. This force creates a moment on the engine, rotating about the engine's CoG, as represented by the cross-section schematic shown in Figure 34.

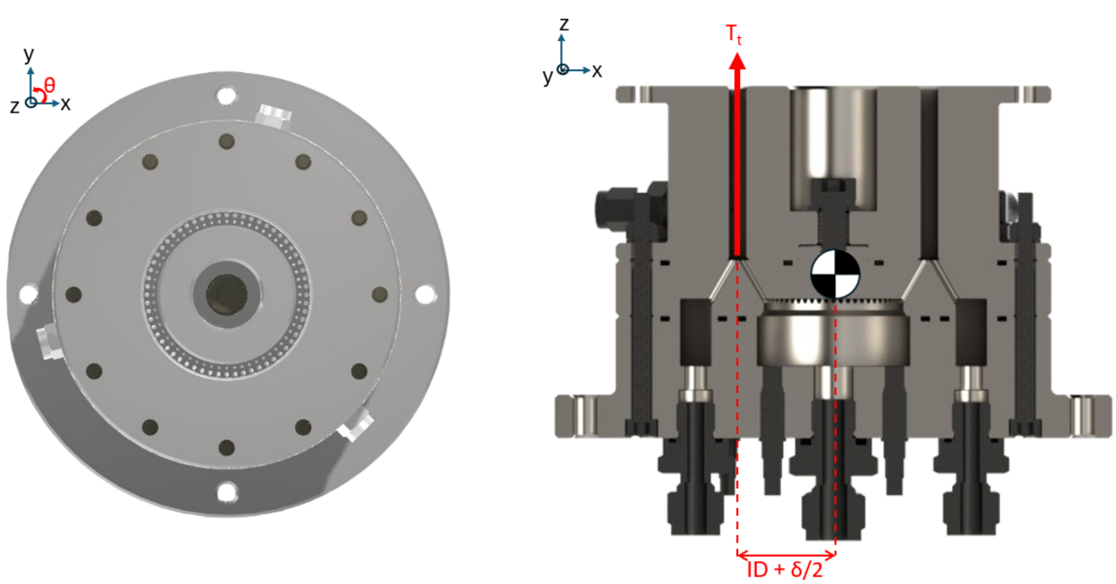

Figure 34: Vectoring Effect in Single Wave Mode

Where ID is inner diameter of the combustion chamber, and δ is the combustion chamber width. Assuming a 2D RDE, symmetric about the Z axis, ignoring reaction moments; the moment created by the eccentric thrust can be shown by Equation 18.

$$+ \circlearrowleft \Sigma M_Y = -T_t * (ID + \frac{\delta}{2}) \tag{18}$$

For the nominal engine designed, assuming an axial thrust of 1350 N, ID of 50 mm, and δ of 5 mm, the instantaneous moment created is:

$$+ \circlearrowleft \Sigma M_Y = -1350 * (50E - 3 + \frac{5E - 3}{2}) = -70.875Nm \tag{19}$$

The instantaneous moment created by the RDE in single wave mode is 74.25Nm, which is counteracted by both the engine's moment of inertia in the Y direction, and thrust stand supports.

In two-wave mode, the thrust vectoring effect is apparently nullified, as the coupled moment cancels, for evenly spaced detonation waves. However, in practice, multiple combustion waves are very difficult to maintain evenly spaced in the azimuth direction.

The XY-plane moment created by N number of co-exiting combustion waves in the cylindrical combustion chamber, for azimuth angle θ is shown in Equation 20.

$$\vec{M_T} = \sum_{i=0}^{N} \vec{M}_i = -F_{ti} Re^{-\theta_i t} \tag{20}$$

Assuming zero rotation about X and Y, the anticipated torque that the torque sensors will experience can be approximated as 70.875Nm.

According to this design, without any counterweights, the axial load cells must be sized for the expected thrust, plus the anticipated weight of all mounted components. As is shown, the expected mass of components mounted above the axial thrust measuring load cells is 10.37 kg as measured from initial CAD. Axial load cells must therefore be sized for minimum load of 1452N.

However, the presented design is not limited in application direction. If the same design were to be mounted on the ceiling, load cells would only need to be sized for 1248N without any counterweights.

Nominal drawings for the preliminary design of this thrust stand are presented in Appendix B.

4.5 Engine Ignition

Engine ignition via DDTT is selected as the most reliable option for achieving rotating detonation [1]. A DDTT at the very core, is simply a PDE applied to an RDE with the sole purpose of promoting directional combustion within the RDE combustion chamber. As discussed in the background information sections, PDEs, like DDTTs are long, slender cylindrical tubes, pre-filled with combustible gas and ignited [1] [84].

The specific objective of DDTTs are slightly different than PDEs due to the application; DDTTs attempt to simply add energy in a primary direction to promote detonation propagation direction. This being said, DDTTs do not necessarily need to be optimized in the way that PDEs for thrust generation. Significant works have been undertaken studying DDTTs as an ignition method for RDEs [11] [51], [43] [85].

Given the time constraints of the early stages of this work, no significant progress has been made with respect to the design of an ignition method beyond choosing the DDTT.

5 Discussions

5.1 Main Engine Performance

5.1.1 Minimum Fill Height

From selected engine design parameters presented in Section 4.1.1.3, an important parameter worth noting is the propellant fill height h^* relative to the combustion chamber length, L. The ratio of h^*/L is 0.7504 for detonation operation in single wave mode, and $h^*/L > 1$ for dual wave combustion mode. Obviously, a fill height exceeding the length of the combustion chamber is not feasible, hence limiting the designed engine to single-wave combustion mode. However, in single-wave combustion mode, a fill height of 75% of the combustion chamber length is high. This has potential to limit the effectiveness and efficiency of the engine by not allowing the oblique shockwave to fully develop before reaching the exit plane. Little known literature investigates the upper bound of combustion parameters with respect to RDE operation, and this was not considered within the time constraints of this engine development. Future works building on this established progress should consider minimum expansion of oblique shock-wave and maximum combustion wave height with respect to engine operational efficacy to better understand the effect of these parameters on engine performance.

5.1.2 Comparison to shared American Engine

Critical engine design parameters are compared to the shared American Engine that is used by Zucrow Laboratories at Purdue, AFRL, University of Central Florida, University of Washington [37], in Table 21.

Table 20: Engine Comparison - Design Parameters

Parameter	Proposed Engine	American Engine [37]
Thrust Target [N]	1350	1350
Designed Specific Impulse [s]	414	-
Mass Flow Rate [g/s]	335	270-375
Outer Diameter [mm]	60	76.2 (3")
Inner Diameter [mm]	50	66.2
Length [mm]	60	76.2
Equivalence Ratio, ϕ	1.0	1.1-1.7
Number of Waves	1	2-3

As shown above in Table 21, the RDE design presented is notably smaller than the American Engine shared among various academic institutions. Considering the combustion chamber size of the American engine, and applying the same critical fill height to thrust logic as presented in Section 4.1.1.2, yields a similar fill height, of 37.5 mm. This equates to a fill height to length ratio, h^*/L of 0.4921, which is significantly lower than the fill height to length ratio of the presented engine, as discussed in Section 5.1.1.

The mass flow rate and equivalence ratio of the proposed engine falls within, or very close to, the experimental operational range of the American engine, indicating that the performance targets are likely similar. Experimental performance results for the American engine are summarized in Table 21.

Table 21: Engine Comparison - Summary of Experimental Performance Results

Parameter	Proposed Engine	American Engine [37]
Thrust Target [N]	1350	1350
Actual Thrust [N]	-	325-625
Actual Specific Impulse [s]	-	150
Number of Waves	1	2-3

It is important to notice the experimental versus designed thrust targets of the American engine; experimental results show an experimental to theoretical thrust ratio between $0.2407 < T_e/T_d < 0.4629$. The low experimental performance of the American engine indicates either a low-efficiency experimental combustion process or an overly optimistic thrust estimation. It is evident that a similar thrust design process is employed by both the proposed engine and the American engine based on the similitude of the propellant feed, and performance predictions. In the engine sizing procedure employed by the proposed engine, there is very little effort to model a realistic combustion system, leading to the tentative conclusion that the idealized system analysis presented is overly optimistic of real combustion processes. Future works should put more emphasis on characterizing combustion losses and inefficiencies throughout the engine system to attempt to close the gap between design and experimental performance results.

5.2 Thrust Stand Design

There are a number of elements not considered in the preliminary thrust stand design presented in Section 4.4. Design over-simplifications, elements earmarked for future analysis, and under-considered components are listed below.

- Vertically downwards versus vertically upwards operation.
- Shaking force analysis.
- Thrust stand leg stiffening.
- Is gravity sufficient for maintaining stationary, upright position of thrust stand?
- Torsion shaft strength and deflection under load analysis.
- Thermal analysis of components adjacent hot-firing engine.
- Modal analysis of thrust frame in comparison to engine operational frequency.

Considering the preliminary nature of the thrust stand design, these elements will not be discussed in further detail. These elements are earmarked for future consideration and are intended to be a representation of the remaining analysis work that could not be finished within the time constraints. This list is by no means exhaustive.

5.3 Future Work

Due to the aggressive nature of the timeline associated with this capstone research project, there are several items that have been under-designed that, given more time, would be the primary focus elements. Items not yet discussed that are earmarked for future development work are listed below;

- Re-design combustion chamber body to avoid operating at resonant frequencies.
- Improve engine sizing approach to include upper bound of feasible combustion energy output.
- Characterizing actual engine operation deviation from ideal analytical model.
- Further comparison against experimental RDEs to predict performance.
- Further investigation into selection of specific sensors (pressure transducers, load cells, etc.).
- Further development of propellant feed system, selecting specific components and developing mounting strategy.
- Perform cold-flow fluid testing of individual components to ensure design flow-rate is attainable.
- Prototype fabrication and testing to better understand operating principles to learn from mistakes.

This list is intended to give a summary of the remaining work the team wishes to complete if sufficient time remained; this list is however, by no means exhaustive.

6 Conclusion

This paper is the culmination of a 16-month capstone project at Memorial University of Newfoundland, Faculty of Engineering and Applied Sciences. Other relevant deliverables throughout this period are available online [86], [87], [88].

The goal of this project was to develop a procedure to size an Rotating Detonation Engine using the currently published research base to help address the analytical modelling of an RDE research gap. It was also sought to yield an experimental RDE prototype for hot-fire testing in the future. Stretch goals for the project were related to validation of the analytical model and theoretical design; complete converting a GH2-Air 2D RDE numerical model to a GH2-GO2 model, and conduct hot-fire testing.

All four team members had distinct technical work to do that was assigned based on each individual's interests and strengths. Collaboration was a staple of the project's progression and working dynamic from its beginning.

Development of the analytical model to generate a theoretical engine design point occurred in MatLab using a set of scripts that drew on first-principles formulations from literature and toolbox plugins. Four calculation functionalities were developed along with two post-processing functionalities. The detonation model scripting is built from functionalities within the Cantera toolbox and the SDToolbox toolbox. Pertinent parameters calculated based on inputs of 130kPa, 300K, equivalence ratio of 1, and propellant of GH2-GO2 are; detonation cell size of 1.2mm, maximum temperature of 3720K, and maximum pressure of 4.3MPa. The minimum geometry, given the detonation thermochemical properties, was calculated using Bykovskii's combustion chamber correlations, which are multiples of the detonation cell size parameter. Due to these minimums not reaching the thrust goal of 1350N, a preliminary geometry originally deemed incorrect was selected. The combustion chamber has an outer diameter of 60mm, an inner diameter of 50mm, a channel width of 5mm, and a length of 50mm. This geometry was still calculated at the time using Bykovskii's correlations. The required fill height, given this geometry and input parameters was recalculated using Bykovskii's correlation to be 37.5mm. Engine performance was calculated using the analytical modelling works of J. E. Shepherd and J. Kasahara. Given the target thrust of 1350N, the mass flow rate required is 334g/s with a specific impulse of 410.7s. The injectors were designed through a two-stage process. Isentropic flow equations were applied to a control volume between the fuel/oxidizer plenums, across the injector plate, and into the combustion chamber to yield a theoretical equivalent injection area that will result in a choked flow condition within the injectors, given pressure requirements in the combustion chamber and pressure estimation in the plenums. The second step was to apply manufacturing constraints to determine the minimum feasible total injection area, and then back-calculate plenum pressures to maintain chamber pressures and choked flow. 60 1mm holes with an area ratio of 5.45% at a plenum pressure of 1.102MPa was determined for Hydrogen feeding, and 60 1.5mm holes with an area ratio of 12.27% at a plenum pressure of 0.9757MPa was determined for Oxygen feeding.

Altair HyperMesh and the OptiStruct solver was used for the entire FEA analyses of this project. The mesh was created semi-manually to accurately reflect the true engine geometric features without adding artificial model stiffness. The resultant mesh was primarily formed from first-order hexahedral elements with minimal amounts of first-order pentahedral elements. Due to the geometry of the engine computationally expensive second-order tetrahedral elements were not required. To represent the 316L-SS material, a linear isotropic material model was selected. Three types of analyses were completed; modal, static thermal, and static pressure. Given the calculated wave frequency of 16.4937kHz, the modal analysis determined that this was within 5Hz of the 40th mode of the engine. Due to an error in original calculation of the wave frequency, it was only determined after selection of the final engine design that there would be operational resonance. The static thermal result was not entirely useful as it is understood the engine cannot operate at steady state conditions due to material failure, therefore the maximum thermal stress of 38GPa does not give useful insight into engine strength but it does reinforce the notion that this engine cannot be run to steady-state conditions. A transient analysis of an operation run time of 1s would have to be done to glean more useful results from a thermal analysis. The static pressure results provide more helpful information. The maximum stress of 16.32MPa is well below the yield strength of 316L stainless indicating that the pressure from the detonation wave is not of concern for the engine's structural integrity.

Two CFD simulations were undertaken during the duration of this project, both using the Convergent Science software CONVERGE CFD. The 2D stoichiometric Hydrogen and Oxygen combustion simulation in its current state shows promising results after extensive work, but a fully functional model has not been finished within the project timeline. By extension, numerical validation of the analytical model was not possible. The second simulation was a 3D non-reactive flow of the propellant injection. The results proved to validate the choking of fuel/oxidizer in their respective injection orifices but demonstrated poor mixing characteristics due to an acceleration past Ma = 1 at the end of the injectors.

The engine is made up of 4 parts, the base plate, injector plate, outer body, and centre body. The alignment between the centre body and the outer body bore is critical for a concentric annular combustion chamber. M6 precision ground dowels are used as locating features. A maximum of 117 microns of misalignment between the centre body OD and outer body bore can exist. These tolerances and misalignments are optimized for manufacturing cost and engine performance. The engine relies on axial O-Ring sealing to seal the fuel and oxidizer plenums from each other and to seal the combustion chamber from exhausting gases between the stacked plates. The O-Rings are nitrile rubber and are compatible with oxygen and hydrogen. The O-Ring features were sized using the Trelleborg Solutions O-Ring calculator. The most pertinent manufacturing instruction will be to machine the bore of the annular combustion chamber after the engine has been assembled with dowels and bolted together.

In the event that further work occurs on this project, there are some specific points that should see further development; Re-design engine to avoid operating near resonant frequencies, improve the analytical model to include design point calculation above the minima and consider system losses, complete development of a propellant feed system, perform cold-flow testing of individual components, and have a prototype fabricated which undergoes hot-fire testing.

Acronyms

AFIT	Air Force Institute of Technology 9
AFRL	Air Force Research Laboratory 9, 36
CAD	Computer Aided Design 13, 35
CalTech	California Institute of Technology 16, 17, 19, IV
CFD	Computational Fluid Dynamics 25–27, 38, I, II, IV
CJ	Chapman Jouguet 7, 8, 16
CMM	Coordinate-Measuring Machine 29
CoG	Center of Gravity 34
CTAP	Capillary Tube Average Pressure 10
DAQ	Data Acquisition 13
DDT	Deflagration-to-Detonation Transition 6
DDTT	Deflagration-to-Detonation Transition Tube 8, 9, 32, 35
DETechnologies	Detonation Engine Technologies 13, 14, 29
DFMA	Design For Manufacturing and Assembly 13, 27, II
DOF	Degree of Freedom 33, 34
FEA	Finite Element Analysis 13, 21–23, 38, I, II, IV
MATS	Multi-Axis Thrust Stand 12
NASA	National Space and Aeronautical Administration 9
NETL	National Energy Technology Laboratory 9
P&ID	Piping and Instrumentation Diagram 9, 32, 33, IV
PDE	Pulse Detonation Engine 5, 6, 9, 35, II, IV
RBE	Rigid Body Element 22, 23
RDE	Rotating Detonation Engine 1, 4–13, 18, 20, 23, 25, 26, 31–37, I, II, IV, V
TRL	Technology Readiness Level 33
UCF	University of Central Florida 9, 36
UW	University of Washington 9, 36
ZND	Zel'dovich, von Neumann and Döring 7, 16

References

[1] I. J. Shaw, J. A. Kildare, M. J. Evans, A. Chinnici, C. A. Sparks, S. N. Rubaiyat, R. C. Chin, and P. R. Medwell, "A theoretical review of rotating detonation engines," *Direct Numerical Simulations-An Introduction and Applications*, 2019.

[2] B. V. Voitsekhovskii, "Detonation combustion of a gas mixture in a cylindrical chamber," *Doklady Akademii Nauk SSSR*, vol. 129, no. 6, 1959.

[3] F. A. Bykovskii and V. V. Mitrofanov, "Detonation combustion of a gas mixture in a cylindrical chamber," *Combustion, Explosion and Shock Waves*, vol. 16, pp. 570–578, Sept. 1980.

[4] D. T. Harrje, *Liquid propellant rocket combustion instability*, vol. 194. Scientific and Technical Information Office, National Aeronautics and Space . . . , 1972.

[5] J. C. Oefelein and V. Yang, "Comprehensive review of liquid-propellant combustion instabilities in f-1 engines," *Journal of Propulsion and Power*, vol. 9, no. 5, pp. 657–677, 1993.

[6] P. Wolański, "Detonative propulsion," *Proceedings of the combustion Institute*, vol. 34, no. 1, pp. 125–158, 2013.

[7] D. L. Chapman, "Vi. on the rate of explosion in gases," *The London, Edinburgh, and Dublin Philosophical Magazine and Journal of Science*, vol. 47, no. 284, pp. 90–104, 1899.

[8] E. Jouguet, "Sur la propagation des réactions chimiques dans les gaz [on the propagation of chemical reactions in gases]," *Journal de Mathématiques Pures et Appliquées*, vol. 60, p. 345, 1905.

[9] K. K. Kuo, "Principles of combustion," 1986.

[10] C. A. Nordeen, "Thermodynamics of a rotating detonation engine," 2013.

[11] S. J. Miller, "Design and testing of an h2/o2 predetonator for a simulated rotating detonation engine channel," 2013.

[12] S. R. Chakravarthy, "Mod-06 lec-26 velocity, temperature and entropy variation along hugoniot curve," Jun 2016.

[13] Y. B. Zel'dovich, " [on the theory of the propagation of detonation in gaseous systems]," *Journal of Experimental and Theoretical Physics*, vol. 10, pp. 542–568, 1940.

[14] J. von Neumann, "Theory of detonation waves," tech. rep., Institute for Advanced Study, 1942.

[15] W. Döring, "Über den detonationsvorgang in gasen [on the detonation process in gases]," *Annalen der Physik*, vol. 435, pp. 421–436, 1943.

[16] K. Pandey, P. Debnath, *et al.*, "Review on recent advances in pulse detonation engines," *Journal of Combustion*, vol. 2016, 2016.

[17] J.-L. Li, W. Fan, C.-J. Yan, H.-Y. Tu, and K.-C. Xie, "Performance enhancement of a pulse detonation rocket engine," *Proceedings of the Combustion Institute*, vol. 33, no. 2, pp. 2243–2254, 2011.

[18] J. Kasahara, A. Hasegawa, T. Nemoto, H. Yamaguchi, T. Yajima, and T. Kojima, "Performance validation of a single-tube pulse detonation rocket system," *Journal of propulsion and power*, vol. 25, no. 1, pp. 173–180, 2009.

[19] L. Barr, "Pulsed detonation engine flies into history." https://www.af.mil/News/Article-Display/Article/123534/pulsed-detonation-engine-flies-into-history/, May 2008. Accessed: 2024-03-01.

[20] G. Rong, M. Cheng, Z. Sheng, X. Liu, and J. Wang, "Investigation of counter-rotating shock wave phenomenon and instability mechanisms of rotating detonation engine with hollow combustor and laval nozzle," *International Journal of Hydrogen Energy*, vol. 47, no. 54, pp. 23019–23037, 2022.

[21] H.-S. Han, E. S. Lee, and J.-Y. Choi, "Experimental investigation of detonation propagation modes and thrust performance in a small rotating detonation engine using c2h4/o2 propellant," *Energies*, vol. 14, no. 5, p. 1381, 2021.

[22] M. L. Fotia, F. Schauer, T. Kaemming, and J. Hoke, "Experimental study of the performance of a rotating detonation engine with nozzle," *Journal of Propulsion and Power*, vol. 32, no. 3, pp. 674–681, 2016.

[23] D. E. Paxson, K. Miki, H. D. Perkins, and S. Yungster, "Computational fluid dynamic optimization of an experimental rotating detonation rocket engine nozzle," in *AIAA AVIATION 2022 Forum*, p. 4107, 2022.

[24] M. Ross, J. Burr, Y. Desai, A. Batista, and C. Lietz, "Flow acceleration in an rdre with gradual chamber constriction," *Shock Waves*, vol. 33, no. 3, pp. 253–265, 2023.

[25] A. Gavrikov, A. Efimenko, and S. Dorofeev, "A model for detonation cell size prediction from chemical kinetics," *Combustion and flame*, vol. 120, no. 1-2, pp. 19–33, 2000.

[26] H. D. Ng, Y. Ju, and J. H. Lee, "Assessment of detonation hazards in high-pressure hydrogen storage from chemical sensitivity analysis," *International Journal of Hydrogen Energy*, vol. 32, no. 1, pp. 93–99, 2007.

[27] C. K. Westbrook and P. A. Urtiew, "Use of chemical kinetics to predict critical parameters of gaseous detonations," *Combustion, Explosion and Shock Waves*, vol. 19, no. 6, pp. 753–766, 1983.

[28] F. A. Bykovskii, S. A. Zhdan, and E. F. Vedernikov, "Continuous spin detonations," *Journal of propulsion and power*, vol. 22, no. 6, pp. 1204–1216, 2006.

[29] R. M. Russo, "Operational characteristics of a rotating detonation engine using hydrogen and air," 2011.

[30] A. P. Nair, A. R. Keller, N. Q. Minesi, D. I. Pineda, and R. M. Spearrin, "Detonation cell size of liquid hypergolic propellants: Estimation from a non-premixed combustor," *Proceedings of the Combustion Institute*, vol. 39, no. 3, pp. 2757–2765, 2023.

[31] J. E. Shepherd and J. Kasahara, "Analytical models for the thrust of a rotating detonation engine," 2017.

[32] P. Wolański, "Rde research and development in poland," *Shock Waves*, vol. 31, no. 7, pp. 623–636, 2021.

[33] F. A. e. Bykovskii, S. A. Zhdan, and E. F. Vedernikov, "Parameters of continuous multifront detonation of a methane mixture with heated air in an annular cylindrical combustor," *Combustion, Explosion, and Shock Waves*, vol. 58, no. 2, pp. 149–158, 2022.

[34] C. A. Nordeen, D. Schwer, A. T. Corrigan, and B. Cetegen, "Radial effects on rotating detonation engine swirl," in *51st AIAA/SAE/ASEE Joint Propulsion Conference*, p. 3781, 2015.

[35] Q. Michalski, R. Aliakbari, N. Mason-Smith, N. Paull, M. Wenzel, and A. Pudsey, "Structure of rotating detonation in mixtures of natural gas and oxygen," *Combustion and Flame*, vol. 260, p. 113253, 2024.

[36] S. F. Connolly-Boutin, M. Ghali, R. Gilot, J. Loiseau, A. J. Higgins, and C. B. Kiyanda, "Initiation dynamics of rotating detonation engines using c2h4-o2 mixtures,"

[37] J. W. Bennewitz, J. R. Burr, B. R. Bigler, R. F. Burke, A. Lemcherfi, T. Mundt, T. Rezzag, E. W. Plaehn, J. Sosa, I. V. Walters, *et al.*, "Experimental validation of rotating detonation for rocket propulsion," *Scientific Reports*, vol. 13, no. 1, p. 14204, 2023.

[38] R. Burke, "Rotating detonation engine injector and method of designing," U.S. Patent 2023/0340931 A1, Oct. 2023.

[39] T. Mundt, *Geometric Scaling of Cylindrical Rotating Detonation Rocket Engine Combustors*. PhD thesis, 2023.

[40] S. Zhou, Y. Ma, F. Liu, and N. Hu, "Experimental investigation on pulse operation characteristics of rotating detonation rocket engine," *Fuel*, vol. 354, p. 129408, 2023.

[41] I. Q. Andrus, "A premixed rotating detonation engine: Design and experimentation," *AIR FORCE INSTITUTE OF TECHNOLOGY WRIGHT-PATTERSON AFB OH WRIGHT-PATTERSON*, 2016.

[42] R. Burke, *Characteristics of Rotating Detonation Engines for Propulsion and Power Generation*. PhD thesis, University of Central Florida, 2022.

[43] J. C. Shank, "Development and testing of a rotating detonation engine run on hydrogen and air," 2012.

[44] J. Z. Ma, S. Zhang, M. Luan, and J. Wang, "Experimental investigation on delay time phenomenon in rotating detonation engine," *Aerospace Science and Technology*, vol. 88, pp. 395–404, 2019.

[45] K. Ishihara, Y. Kato, K. Matsuoka, J. Kasahara, A. Matsuo, and I. Funaki, "Thrust performance evaluation of a rotating detonation engine with a conical plug," in *25th International Colloquium on the Dynamics of Explosions and Reactive Systems, Leeds, UK*, 2015.

[46] W. Saul and M. C. Grubelich, "Rocket engine test system for development of novel propulsion technologies.," tech. rep., Sandia National Lab.(SNL-NM), Albuquerque, NM (United States), 2016.

[47] J. Kindracki, P. Wolański, and Z. Gut, "Experimental research on the rotating detonation in gaseous fuels–oxygen mixtures," *Shock waves*, vol. 21, pp. 75–84, 2011.

[48] K. Goto, Y. Kato, K. Ishihara, K. Matsuoka, J. Kasahara, A. Matsuo, I. Funaki, D. Nakata, K. Higashino, and N. Tanatsugu, "Thrust validation of rotating detonation engine system by moving rocket sled test," *Journal of Propulsion and Power*, vol. 37, no. 3, pp. 419–425, 2021.

[49] Q. Xie, Z. Ji, H. Wen, Z. Ren, P. Wolanski, and B. Wang, "Review on the rotating detonation engine and it's typical problems," *Transactions on Aerospace Research*, vol. 2020, no. 4, pp. 107–163, 2020.

[50] R. F. Burke, T. Rezzag, and K. A. Ahmed, "Validation of experimental evidence for h2/o2 powered rotating detonation rocket engine," in *AIAA Propulsion and Energy 2021 Forum*, p. 3672, 2021.

[51] M. Fotia, J. Hoke, and F. Schauer, "Study of the ignition process in a laboratory scale rotating detonation engine," *Experimental Thermal and Fluid Science*, vol. 94, pp. 345–354, 2018.

[52] A. C. St. George, R. B. Driscoll, D. E. Munday, and E. J. Gutmark, "Development of a rotating detonation engine facility at the university of cincinnati," in *53rd AIAA Aerospace Sciences Meeting*, p. 0635, 2015.

[53] L. Peng, D. Wang, X. Wu, H. Ma, and C. Yang, "Ignition experiment with automotive spark on rotating detonation engine," *International Journal of Hydrogen Energy*, vol. 40, no. 26, pp. 8465–8474, 2015.

[54] F. A. e. Bykovskii, S. A. Zhdan, and E. F. Vedernikov, "Initiation of detonation of fuel-air mixtures in a flow-type annular combustor," *Combustion, Explosion, and Shock Waves*, vol. 50, pp. 214–222, 2014.

[55] J. Nlcholls, R. E. CULLEN, and K. Ragland, "Feasibility studies of a rotating detonation wave rocket motor.," *Journal of Spacecraft and Rockets*, vol. 3, no. 6, pp. 893–898, 1966.

[56] M. Lightfoot, S. A. Danczyk, J. Watts, and S. Schumaker, "Accuracy and best practices for small-scale rocket engine testing," in *JANNAF 2011 Joint Subcommittee Meeting*, 2011.

[57] B. S. Hermannsson, "Development and analysis of a gaseous hydrogen-oxygen rotating detonation combustor," 2022.

[58] J. L. Kerrebrock, A. Epstein, D. Haines, and W. Thompkins, "The mit blowdown compressor facility," 1974.

[59] S. F. Connolly-Boutin, *Detonation Physics-Based Modelling & Design of a Rotating Detonation Engine.* PhD thesis, Concordia University, 2019.

[60] A. Roy, P. Strakey, T. Sidwell, and D. H. Ferguson, "Unsteady heat transfer analysis to predict combustor wall temperature in rotating detonation engine," in *51st AIAA/SAE/ASEE joint propulsion conference*, p. 4191, 2015.

[61] A. M. Begishev, V. Y. Zhuravlev, and A. S. Torgashin, "Features and modernization methods of thrust measurement devices for liquid rocket engine test stands," , vol. 21, no. 1, pp. 62–69, 2020.

[62] R. F. Burke, T. Rezzag, A. Rodriguez, K. Garcia, K. A. Ahmed, and A. Kotler, "Development of an automatic-calibrating small-scale thrust stand for rotating detonation rocket engines," in *AIAA SciTech 2022 Forum*, p. 2370, 2022.

[63] T. J. Eberhart, *Static Stand for Measuring Thrust of Solid Rocket Engines and CFD Analysis of Rocket Motor Nozzles.* PhD thesis, North Carolina Agricultural and Technical State University, 2023.

[64] U. Jain, H. Shukla, S. Kapoor, A. Pandey, and H. Nirwal, "Design and analysis of 2-axis rocket motor stand for thrust vectoring," in *AIAA propulsion and energy 2020 forum*, p. 3920, 2020.

[65] Z. Jun, M. A. Akbar, and W. Xin lei, "Optimization of design and measurement principle of six-components force/thrust measurement stand," *Journal of Engineering, Design and Technology*, vol. 18, no. 5, pp. 1371–1379, 2020.

[66] R. N. Rezende, L. R. Alves, A. Mishra, H. Shukla, H. Varshney, H. Dhawan, S. Kapoor, U. Jain, and R. Mendonsa, "Designing a thrust vector test stand for the turborocket," in *AIAA Propulsion and Energy 2021 Forum*, p. 3350, 2021.

[67] T. W. Carpenter, E. W. Blattner, R. E. Stagner, J. Contreras, D. Lencioni, and G. Mcintosh, "Design and evaluation of thrust vectored nozzles using a multicomponent thrust stand," tech. rep., 1990.

[68] C. L. Journell, R. M. Gejji, I. V. Walters, A. I. Lemcherfi, C. D. Slabaugh, and J. B. Stout, "High-speed diagnostics in a natural gas–air rotating detonation engine," *Journal of Propulsion and Power*, vol. 36, no. 4, pp. 498–507, 2020.

[69] C. A. Stevens, M. Fotia, J. Hoke, and F. Schauer, "Comparison of transient response of pressure measurement techniques with application to detonation waves," in *53rd AIAA Aerospace Sciences Meeting*, p. 1102, 2015.

[70] A. Naples, J. Hoke, J. Karnesky, and F. Schauer, "Flowfield characterization of a rotating detonation engine," in *51st AIAA aerospace sciences meeting including the new horizons forum and aerospace exposition*, p. 278, 2013.

[71] J.-P. Wang, S.-B. Yao, and X.-D. Han, "Continuous detonation engine researches at peking university," *Detonation Control for Propulsion: Pulse Detonation and Rotating Detonation Engines*, pp. 161–182, 2018.

[72] D. G. Goodwin, H. K. Moffat, I. Schoegl, R. L. Speth, and B. W. Weber, "Cantera: An object-oriented software toolkit for chemical kinetics, thermodynamics, and transport processes." `https://www.cantera.org`, 2023. Version 3.0.0.

[73] S. T. Browne and J. Ziegler, "Numerical solution methods for shock and detonation jump conditions," 2004.

[74] S. Browne, J. Ziegler, and J. E. Shepherd, "Shock and detonation toolbox - 2021 version," Feb 2023.

[75] M. Kaneshige and J. E. Shepherd, "Detonation database," 1997.

[76] S. Washko and G. Aggen, "Wrought Stainless Steels," in *Properties and Selection: Irons, Steels, and High-Performance Alloys*, ASM International, 01 1990.

[77] "316 stainless steel, annealed bar." `https://www.matweb.com/search/DataSheet.aspx?MatGUID=dfced4f11d63459e8ef8733d1c7c1ad2&ckck=1`. Accessed: 2023-01-16.

[78] P. M. Knupp, "Algebraic mesh quality metrics," *SIAM journal on scientific computing*, vol. 23, no. 1, pp. 193–218, 2001.

[79] K.-H. Yang, *Basic finite element method as applied to injury biomechanics.* Academic Press, 2017.

[80] K. Richards, P. Senecal, and E. Pomraning, *CONVERGE 3.1.* Madison, WI: Convergent Science, 2024.

[81] International Organization for Standardization, *Geometrical Product Specifications (GPS) - ISO Code System for Tolerances on Linear Sizes - Part 2: Tables of Standard Tolerance Grades and Limit Deviations for Holes and Shafts*, 2010.

[82] "Trelleborg solutions o-ring calculator." `https://www.trelleborg.com/en/seals/resources/design-support-and-engineering-tools/o-ring-calculator`. Accessed: 2023-01-21.

[83] J. John and T. Keith, *Gas Dynamics.* Pearson Prentice Hall, 2006.

[84] Z.-J. Xia, Z.-H. Sheng, D.-W. Shen, and J.-P. Wang, "Numerical investigation of pre-detonator in rotating detonation engine," *International Journal of Hydrogen Energy*, vol. 46, no. 61, pp. 31428–31438, 2021.

[85] J. Nielsen, C. Stevens, P. King, F. Schauer, and J. Hoke, "Detonation propagation through ducts in a pulsed detonation engine," in *49th AIAA aerospace sciences meeting including the new horizons forum and aerospace exposition*, p. 585, 2011.

[86] S. Miri, L. Palmer, A. Clark, P. Cleary, and X. Duan, "Hydrogen-oxygen rotating detonation rocket engine development," 2023.

[87] S. Miri, L. Palmer, A. Clark, P. Cleary, and N. Ryan, "The launch canada-initial design proposal detechnologies memorial university of newfoundland and labrador," 2023.

[88] S. Miri, L. Palmer, A. Clark, P. Cleary, and X. Duan, "Detechnologies midterm report memorial university of newfoundland and labrador me 8705-mechanical engineering capstone ii," 2024.

A Detailed Engine Manufacturing and Assembly Drawings

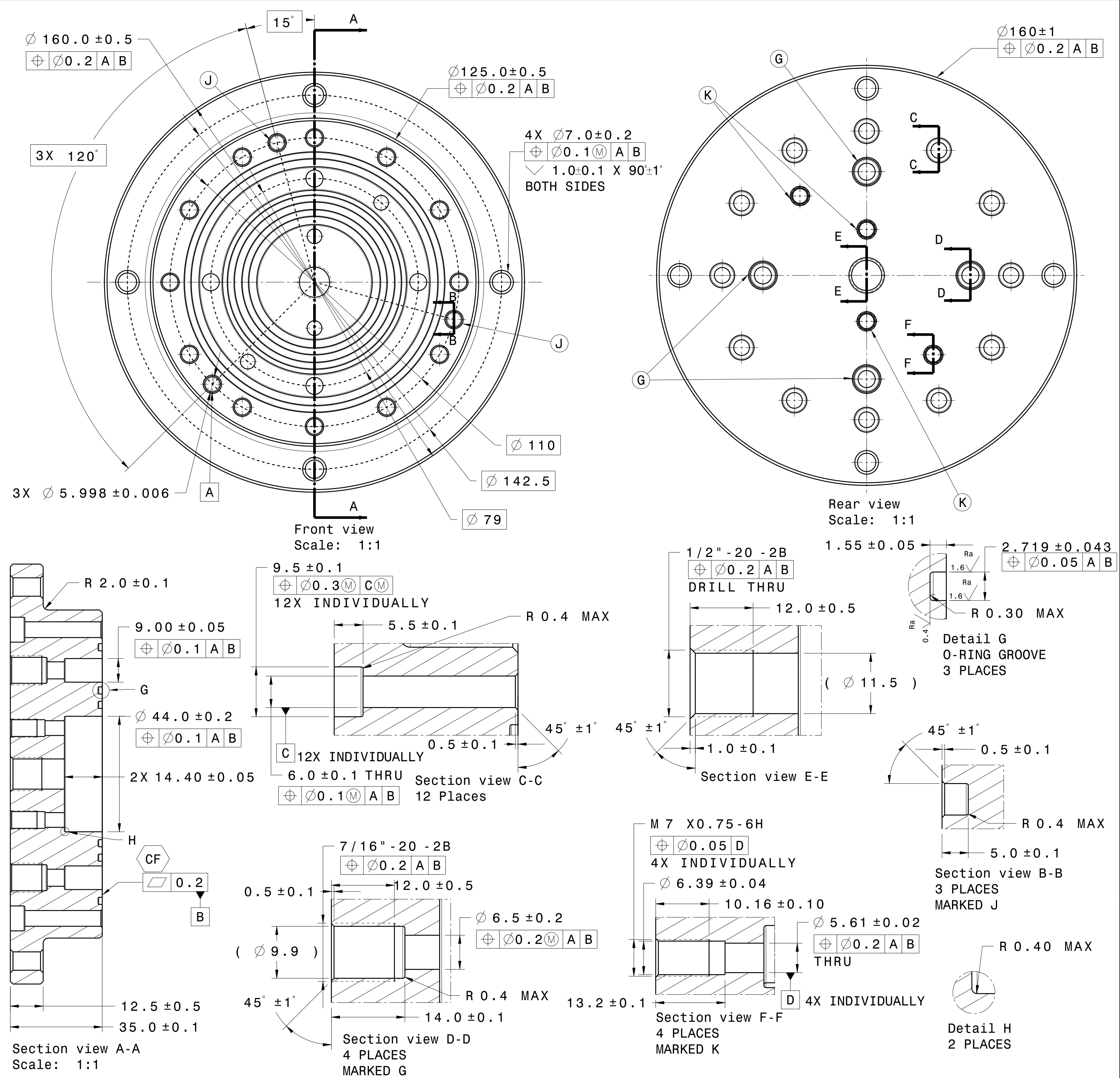

REV	DATE	DESCRIPTION	DRW	APV
A	2024-04-03			

GENERAL

G1. DO NOT SCALE FROM DRAWING
G2.

DIMENSIONS

D1. DIMENSIONS ARE IN MM.
D2. INTERPRET DRAWING PER ASME Y14.5M-2018.
D2. TOLERANCES: UNLESS OTHERWISE SPECIFIED.

⌓ 0.5 | A | B | C

MATERIAL SPECIFICATION

M1. SURFACE FINISH: Ra 3.2 UNLESS OTHERWISE SPECIFIED.
M2. BREAK ALL SHARP EDGES 0.4MM

PROPRIETARY AND CONFIDENTIAL

DETechnologies

DRAWING TITLE: BASE PLATE		
DRAWN BY: P.CLEARY	DATE: 2024-04-03	DRAWING NUMBER: 001-00-A
SIZE: C	MATERIAL: 316 STAINLESS	REV: A
SCALE: NTS	WEIGHT(g): XXX	SHEET: 1/1

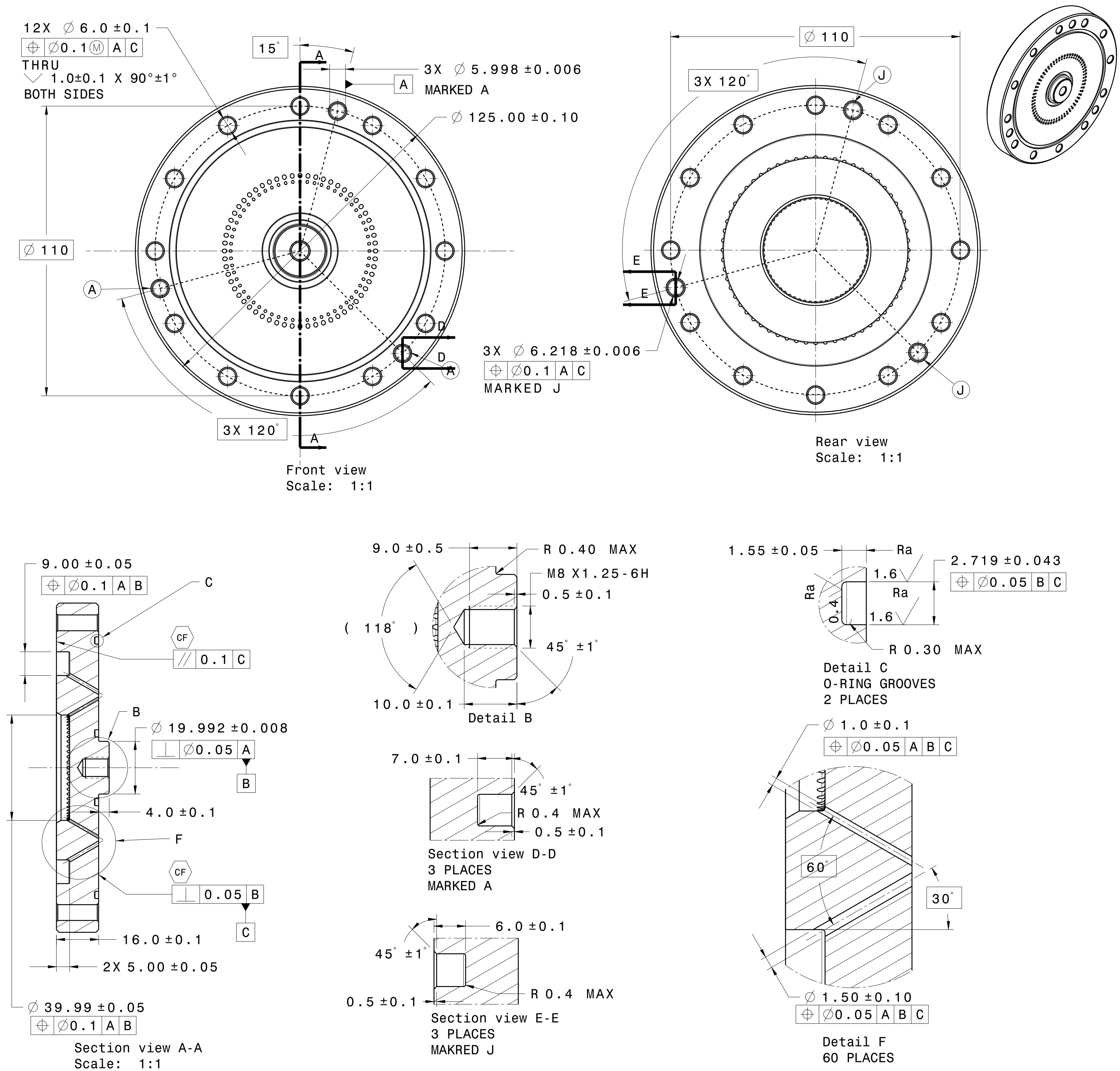

REV	DATE	DESCRIPTION	DRW	APV
A	2024-04-03			

GENERAL

G1. DO NOT SCALE FROM DRAWING
G2.

DIMENSIONS

D1. DIMENSIONS ARE IN MM.
D2. INTERPRET DRAWING PER ASME Y14.5M-2018.
D2. TOLERANCES: UNLESS OTHERWISE SPECIFIED.

⌓ 0.5 A B

MATERIAL SPECIFICATION

M1. SURFACE FINISH: Ra 3.2 UNLESS OTHERWISE SPECIFIED.
M2. BREAK ALL SHARP EDGES 0.4MM

PROPRIETARY AND CONFIDENTIAL

DETechnologies

DRAWING TITLE: INJECTOR PLATE		
DRAWN BY: P.CLEARY	DATE: 2024-04-03	DRAWING NUMBER: 001-00-A
SIZE: C	MATERIAL: 316 STAINLESS STEEL	REV: X
SCALE: NTS	WEIGHT(g): XXX	SHEET: 1/1

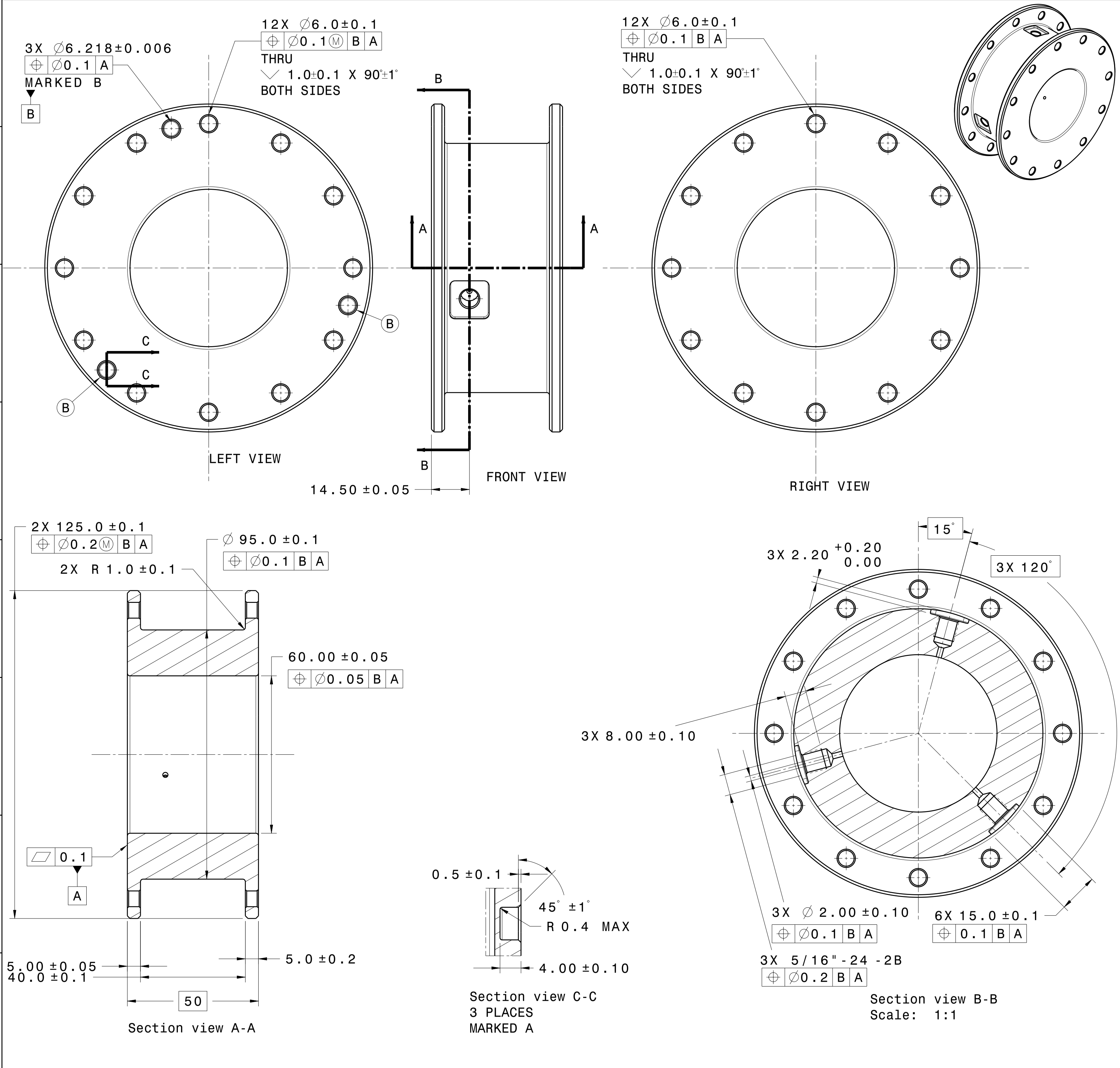

REV	DATE	DESCRIPTION	DRW	APV
A	2024-04-04			

GENERAL

G1. DO NOT SCALE FROM DRAWING
G2.

DIMENSIONS

D1. DIMENSIONS ARE IN MM.
D2. INTERPRET DRAWING PER ASME Y14.5M-2018.
D2. TOLERANCES: UNLESS OTHERWISE SPECIFIED.

⌓ 0.5 | A | B | C

MATERIAL SPECIFICATION

M1. SURFACE FINISH: Ra 3.2 UNLESS OTHERWISE SPECIFIED.
M2. BREAK ALL SHARP EDGES 0.4MM

PROPRIETARY AND CONFIDENTIAL

DETechnologies

DRAWING TITLE	OUTER BODY	
DRAWN BY: P.CLEARY	DATE: 2024-04-03	DRAWING NUMBER: 002-00-A
SIZE: C	MATERIAL: 316 STAINLESS STEEL	REV: A
SCALE: N.T.S	WEIGHT(g): XXX	SHEET: 1/1

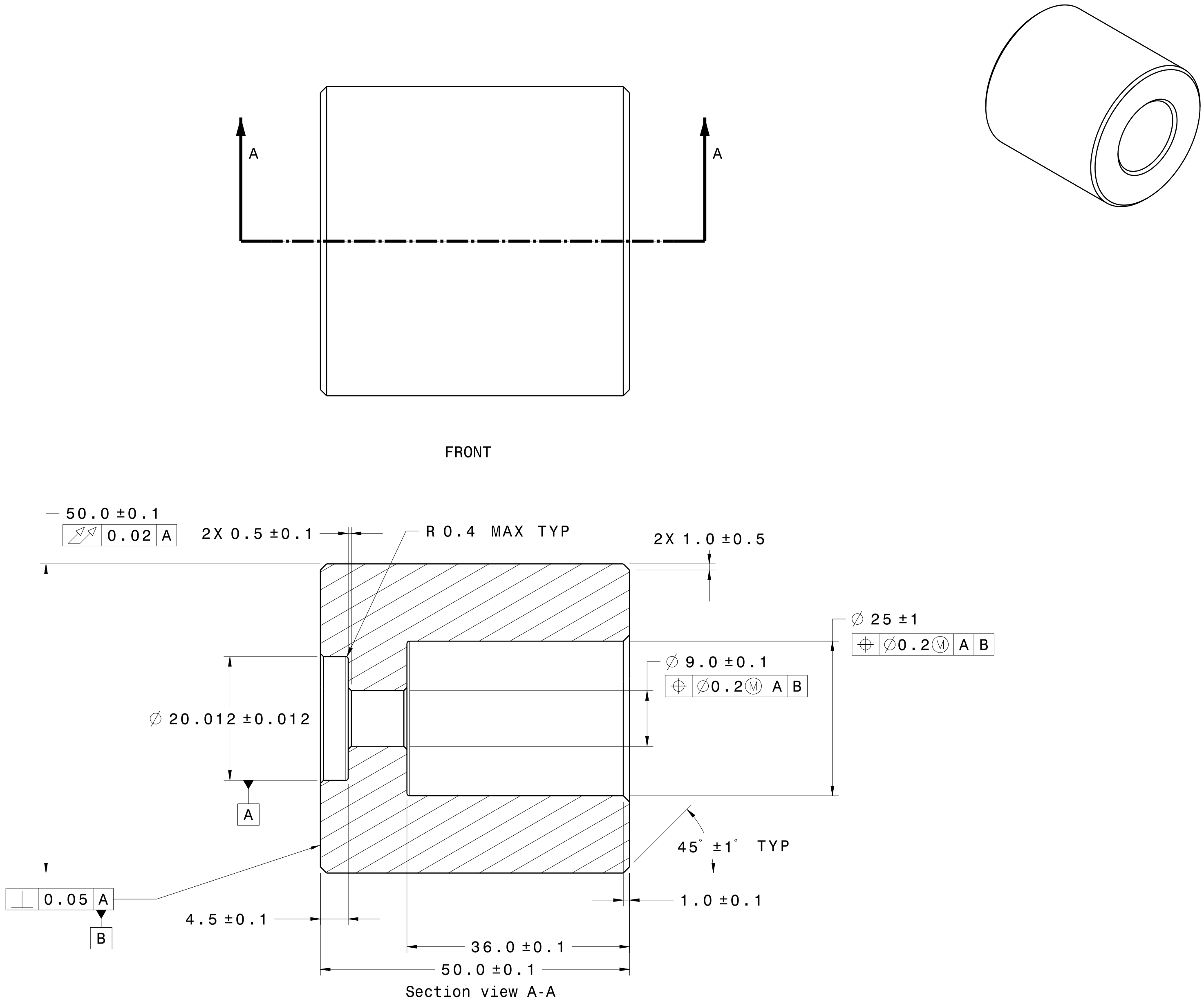

REV	DATE	DESCRIPTION	DRW	APV
A	2024-03-04			

GENERAL

G1. DO NOT SCALE FROM DRAWING
G2.

DIMENSIONS

D1. DIMENSIONS ARE IN MM.
D2. INTERPRET DRAWING PER ASME Y14.5M-2018.
D2. TOLERANCES: UNLESS OTHERWISE SPECIFIED.

⌓ 0.5 | A | B | C

MATERIAL SPECIFICATION

M1. SURFACE FINISH: Ra 3.2 UNLESS OTHERWISE SPECIFIED.
M2. BREAK ALL SHARP EDGES 0.4MM

PROPRIETARY AND CONFIDENTIAL

DETechnologies

DRAWING TITLE: CENTER BODY			
DRAWN BY: P.CLEARY	DATE: 2024-03-04	DRAWING NUMBER: 004-00-A	
SIZE: C	MATERIAL: 316 STAINLESS STEEL		REV: A
SCALE N.T.S	WEIGHT(g) XXX	SHEET 1/1	

#	PART #	DESCRIPTION	QUANTITY
1	001-000-A	BASE PLATE	1
2	002-00-A	INJECTOR PLATE	1
3	003-00-A	OUTER BODY	1
4	004-00-A	CENTER BODY	1

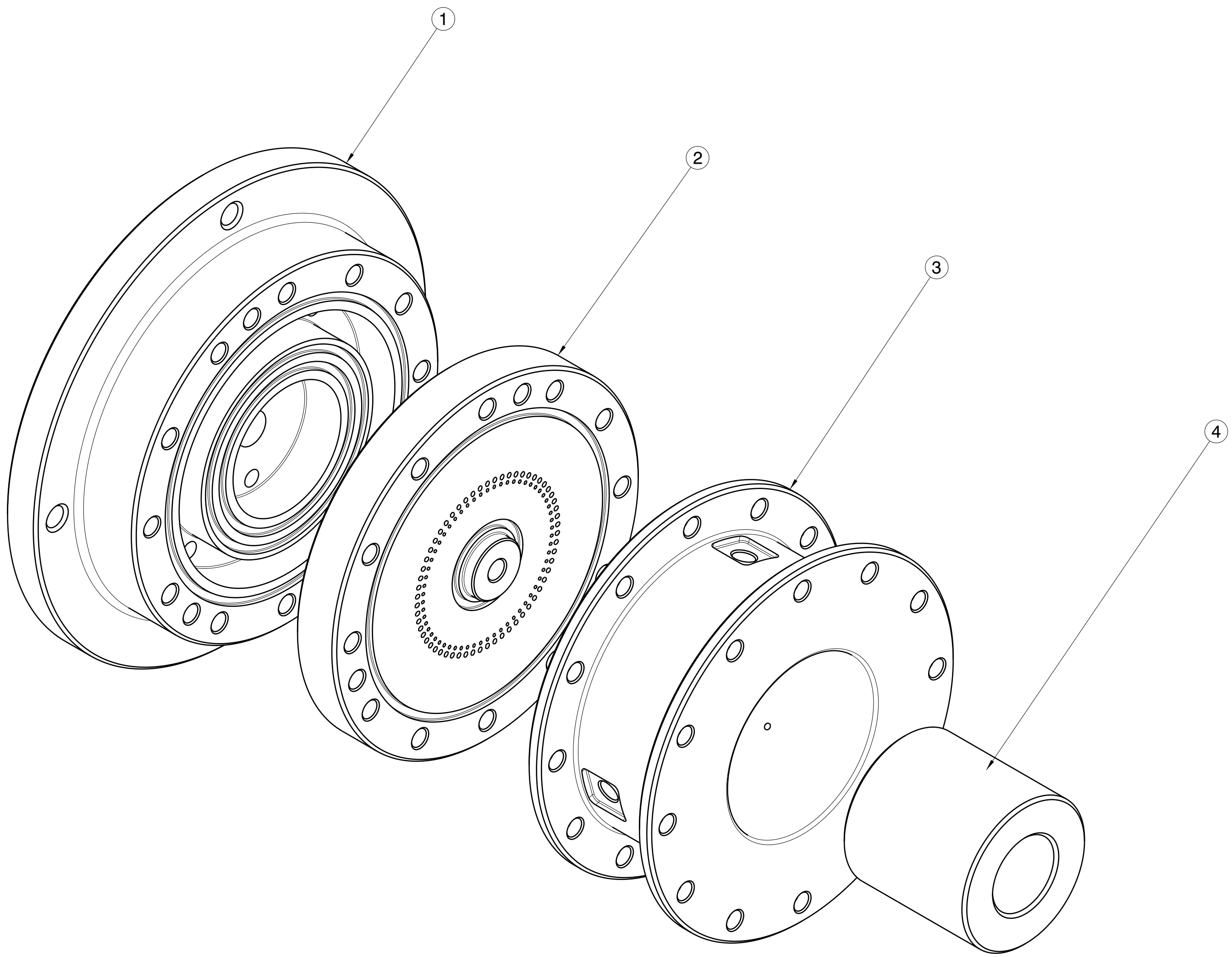

REV	DATE	DESCRIPTION	DRW	APV
A	2024-04-03			

GENERAL

G1.
G2.

DIMENSIONS

D1. DIMENSIONS ARE IN MM.
D2. INTERPRET DRAWING PER ASME Y14.5M-2018.
D2. TOLERANCES: UNLESS OTHERWISE SPECIFIED.

⌓ | 0.5 | A | B | C

MATERIAL SPECIFICATION

M1. SURFACE FINISH: Ra 3.2 UNLESS OTHERWISE SPECIFIED.
M2. BREAK ALL SHARP EDGES 0.4MM

PROPRIETARY AND CONFIDENTIAL

DETechnologies

DRAWING TITLE		
RDE ASSEMBLY DRAWING		
DRAWN BY: P.CLEARY	DATE: 2024-04-03	DRAWING NUMBER: 005-00-A
SIZE: C	MATERIAL: STAINLESS STEEL	REV: A
SCALE N.T.S	WEIGHT(g) XXX	SHEET 1/1

B Preliminary Nominal Drawings of Thrust Stand Design

Credit to L. Heath, DETechnologies' co-op student for the Winter 2024 semester for the following preliminary drawing package of the thrust stand. For academic purposes, since this portion of the project is not considered within the academic scope of deliverables, these drawings are not to be graded.

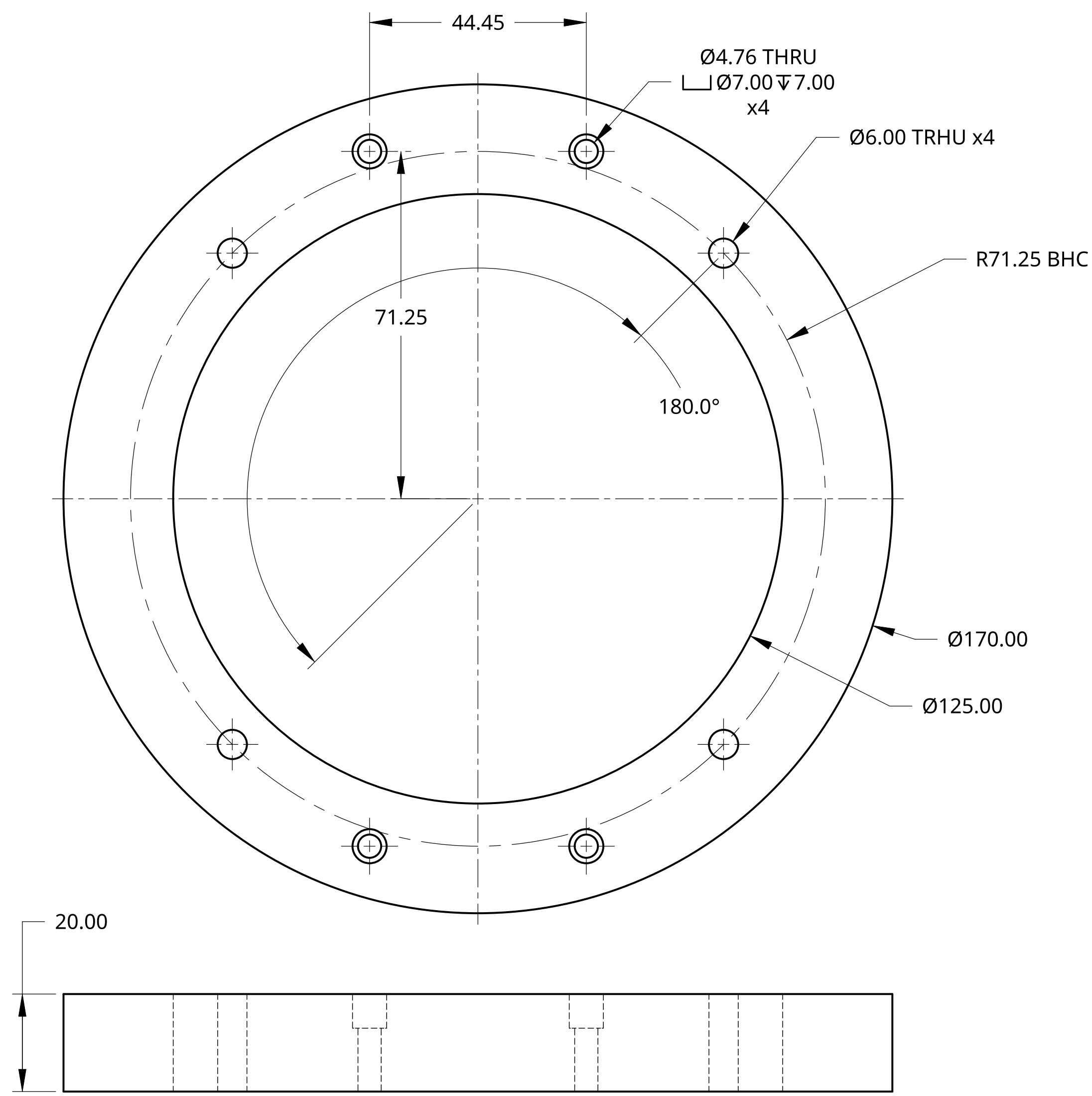

PRELIMINARY DRAWING

MATERIAL	UNLESS OTHERWISE SPECIFIED, DIMENSIONS ARE IN MILIMETERS .XX = ±.0- .XXX = ±.00- .XXXX = ±.000- ANGULAR = ± ° FRACTIONAL = ±	DO NOT SCALE DRAWING		NAME	DATE	Thrust Stand Plate 1
FINISH ---	SURFACE FINISH	BREAK ALL SHARP EDGES AND REMOVE BURRS	DRAWN	LANDYN HEATH	03/25/2024	SIZE B / WEIGHT
		THIRD ANGLE PROJECTION	CHECKED			SCALE 1:1 / SHEET 1 of 4 / REV.
			APPROVED			QTY:

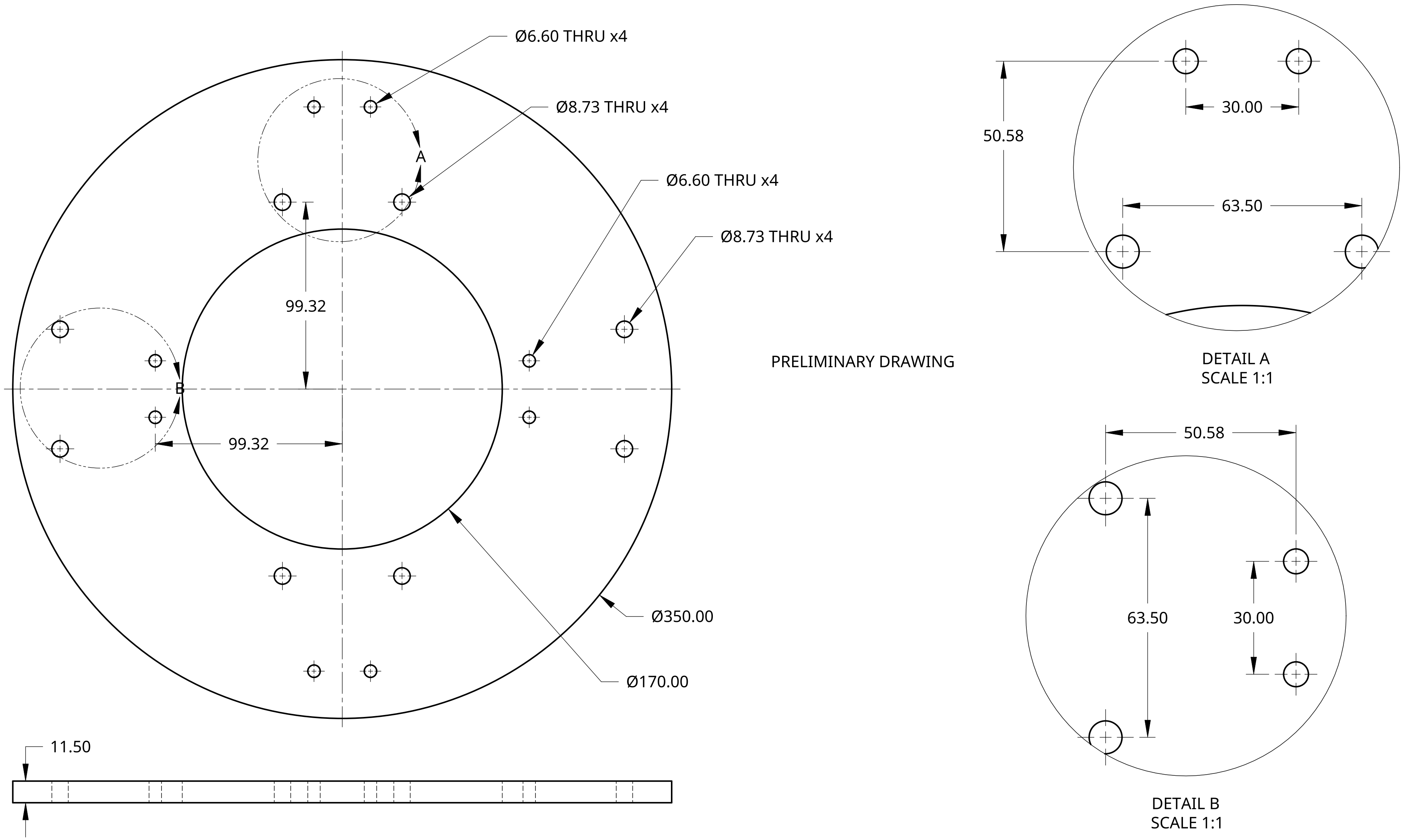

PRELIMINARY DRAWING

MATERIAL	UNLESS OTHERWISE SPECIFIED, DIMENSIONS ARE IN MILIMETERS .XX = ±.0- .XXX = ±.00- .XXXX = ±.000- ANGULAR = ± ° FRACTIONAL = ±	DO NOT SCALE DRAWING		NAME	DATE	THRUST STAND PLATE 2	QTY:
		BREAK ALL SHARP EDGES AND REMOVE BURRS	DRAWN	LANDYN HEATH	03/25/2024	SIZE B	WEIGHT
FINISH ---	SURFACE FINISH	THIRD ANGLE PROJECTION	CHECKED				
			APPROVED			SCALE 1:2	SHEET 2 of 4 REV.

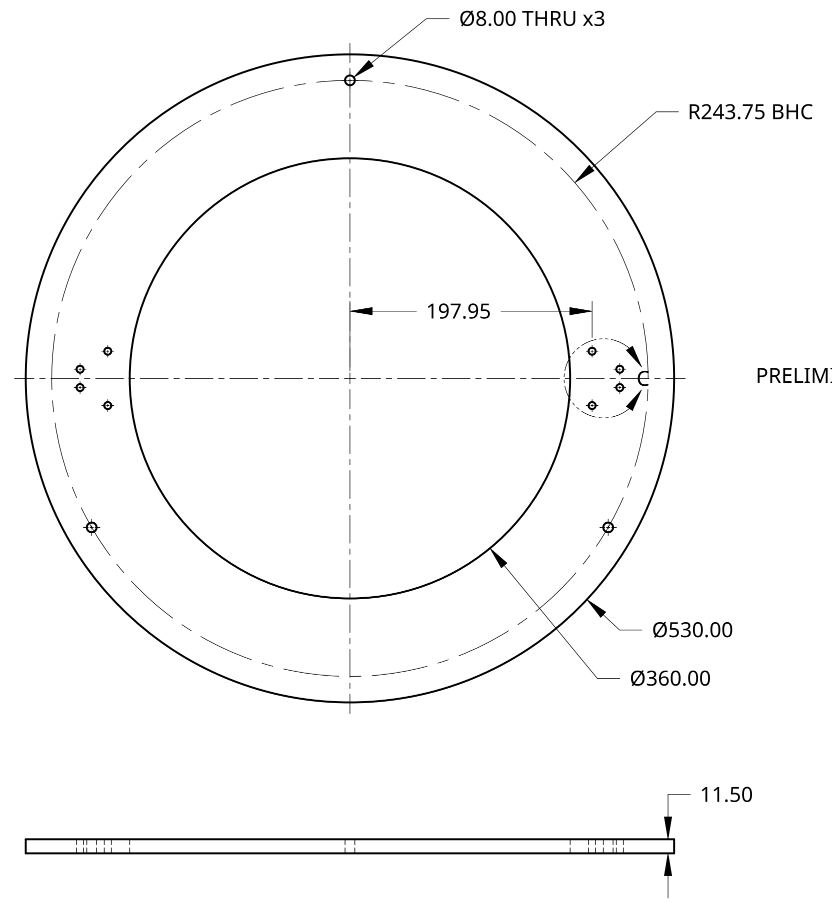

PRELIMINARY DRAWING

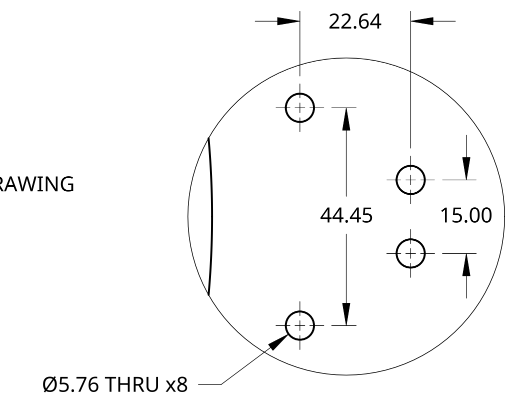

DETAIL C
SCALE 1:1

MATERIAL	UNLESS OTHERWISE SPECIFIED, DIMENSIONS ARE IN MILIMETERS .XX = ±.0- .XXX = ±.00- .XXXX = ±.000- ANGULAR = ± ° FRACTIONAL = ±	DO NOT SCALE DRAWING		NAME	DATE	THRUSTSTAND PLATE 3
		BREAK ALL SHARP EDGES AND REMOVE BURRS	DRAWN	LANDYN HEATH	03/25/2024	SIZE B · WEIGHT
FINISH ---	SURFACE FINISH	THIRD ANGLE PROJECTION	CHECKED			SCALE 1:4 · SHEET 3 of 4 · REV.
			APPROVED			

QTY:

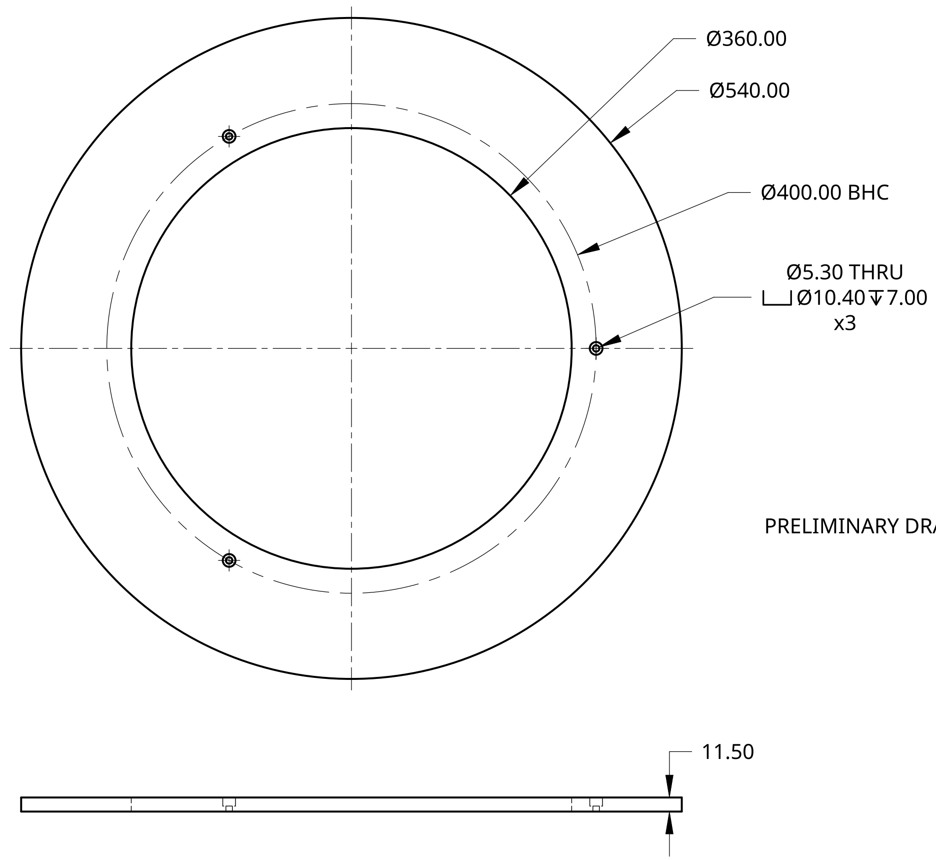

PRELIMINARY DRAWING

MATERIAL	UNLESS OTHERWISE SPECIFIED, DIMENSIONS ARE IN MILIMETERS .XX = ±.0- .XXX = ±.00- .XXXX = ±.000- ANGULAR = ± ° FRACTIONAL = ±	DO NOT SCALE DRAWING		NAME	DATE	THRUST STAND PLATE 4
		BREAK ALL SHARP EDGES AND REMOVE BURRS	DRAWN	LANDYN HEATH	03/25/2024	SIZE B
FINISH ---	SURFACE FINISH	THIRD ANGLE PROJECTION	CHECKED			WEIGHT
			APPROVED			SCALE 1:4 SHEET 4 of 4 REV.

QTY:

C Analytical Models Matlab Codes

C.1 Analytical Model Engine

```
function [gas1,vN_Point,CJ,ZND,CellSizePredictions,Misc,
   GeometryPredictor] = NewAnalyticalModel(P1,T1,eq,mech,
   Bykovskii_adder,CellCorr2Use,GeometryRule,PrintThings)
% Bykovskii_adder: [-5:+5]
%       This drives the 12+5 Bykovskii relation. Used in both
   Bykovskii
%       geometry relations and Nair geometry relations (which are
   derived
%       from Bykovskii)
% CellCorr2Use one of these NUMBERS {'Gavrikov','Westbrook','Ng','
   SeanCB'}=1,2,3,4
%       This is only used in the thrust correlations - we need to know
    what
%       cell size param to grab, because its not really worth
   calculating
%       all of them. A potential future improvement is adding this
   into the
%       geometry calculating loop.
% Geometry rule; 0=nair, 1=bykovskii
%       This is only used in the thrust correlations - we need to know
    what
%       cell size param to grab, because its not really worth
   calculating
%       all of them. A potential future improvement is adding this
   into the
%       geometry calculating loop.
% Print things 1/0
%       print output things to look at. Boolean.

troubleshooting=0%dont hide this line o/p --> failsafe
if troubleshooting
    %Need to make this a matlab script, rather than fcn (comment top
       line)
    %this inits some params to get some values
    clear
    P1 = 180e+3; % [Pa]
    T1 = 300;% [K]
    eq = 1.0;
    mech = 'Burke2012.yaml';
    CellCorr2Use=4
    GeometryRule=0
    PrintThings=1
end

% Theory, numerical methods and applications are described in the
   following report:
%
%     Numerical Solution Methods for Shock and Detonation Jump
   Conditions, S.
%     Browne, J. Ziegler, and J. E. Shepherd, GALCIT Report FM2006.006
    - R3,
%     California Institute of Technology Revised September, 2018.
```

```
%% Initial State (pre-combustion) - State 1 (one)
CellCorr2Use = CellCorr2Use*2;
gas1 = Solution(mech);
eq = InitialState(T1,P1,eq,gas1); % mol ratio of fuel:ox
FAR = sprintf('H2:%d O2:%d',eq(1,1),eq(2,1)); % Fuel:Oxidizer mol
   ratio in string
P_a = 101.325e+3; %P_atm in Pa

%% Calculating combustion parameters to be used later
% Calculating VN Point
vN_Point = vN_State(P1, T1, FAR, mech, gas1,PrintThings);
% Calculating CJ
CJ = CJ_State(P1, T1, FAR, mech, gas1,PrintThings);
% Calculating ZND
ZND = ZND_Structure(P1, T1, FAR, mech, gas1,PrintThings); % all cell
   sizes in [m]
% Sean Conolly-Boutin Additions
SeanCB_CellSize = ((1.6e-3*101.325e+3)/P1); % [m]
CellSizePredictions = table(ZND(22),29*ZND(18),ZND(21),SeanCB_CellSize
   ,'VariableNames',{'Gavrikov','Westbrook','Ng','SeanCB'});

%% Geometry
% Methods:
% F. A. Bykovskii, S. A. Zhdan, and E. F. Vedernikov, "Continuous spin
    detonations,    Journal of propulsion and power, vol. 22, no. 6,
   pp. 1204  1216  , 2006
% A. P. Nair, A. R. Keller, N. Q. Minesi, D. I. Pineda, and R. M.
   Spearrin, "Detonation cell size of liquid hypergolic propellants:
   Estimation from a non-premixed combustor," Proceedings of the
   Combustion Institute, vol. 39, no. 3, pp. 2757  2765  , 2023.
if ~ exist("Bykovskii_adder",'var')
    Bykovskii_adder = 0; % this is the 12+5 thing
end
for i=1:size(CellSizePredictions,2)
    %each loop adds two rows.
    NewR=table([{sprintf('Bykovskii (12+%f)',Bykovskii_adder)};{
       sprintf('Nair (12+%f)',Bykovskii_adder)}],... %Bykovskii/Nair
       rows
        [CellSizePredictions.Properties.VariableNames(1,i);
           CellSizePredictions.Properties.VariableNames(1,i)],... %
           adds cell size predictor name (westbrook/SeanCB/Gavrikov
        [CellSizePredictions{1,i};CellSizePredictions{1,i}],... % cell
            size in both cols (according to loop)
        [(12+Bykovskii_adder)*CellSizePredictions{1,i};(12+
           Bykovskii_adder)*CellSizePredictions{1,i}],... % Min fill
           height
        [28*CellSizePredictions{1,i};40*CellSizePredictions{1,i}],...
           % min OD
        [((12+Bykovskii_adder)/5)*CellSizePredictions{1,i};2.4*
           CellSizePredictions{1,i}],... %min delta (channel width)
        [2*(12+Bykovskii_adder)*CellSizePredictions{1,i};24*
           CellSizePredictions{1,i}],... % min length
        [(12+Bykovskii_adder)*CellSizePredictions{1,i}*((12+
           Bykovskii_adder)/5)*CellSizePredictions{1,i}*(density(gas1)
           )*CJ(1,1);(12+Bykovskii_adder)*CellSizePredictions{1,i
```

```
        }*2.4*CellSizePredictions{1,i}*(density(gas1))*CJ(1,1)],...
      'VariableNames',{'GeometryCorrelations','CellSizePredictor','
        CellSize','MinFillHeight','MinChannelOD','MinChannelWidth',
        'MinChannelLength','Mass Flow Rate kg/s'});

    if i==1
        GeometryPredictor=NewR;
    else
       GeometryPredictor=[GeometryPredictor;NewR];
    end
end

%% Some Sean Things
R_sp = 8.314462618;
Wave_Number_Sean = (GeometryPredictor{CellCorr2Use-GeometryRule,'Mass
   Flow Rate kg/s'}*R_sp*T1)/((12+Bykovskii_adder)*0.0016*101325*CJ
   (1,1)*GeometryPredictor{CellCorr2Use-GeometryRule,'MinFillHeight'})
   ;
Mean_Channel_Diam = GeometryPredictor{CellCorr2Use-GeometryRule,'
   MinChannelOD'}-GeometryPredictor{CellCorr2Use-GeometryRule,'
   MinChannelWidth'};
Fill_Time_Sean = (pi*(Mean_Channel_Diam))/(CJ(1,1)*Wave_Number_Sean);

%% Thrust Calcs
q_h = ((soundspeed_fr(gas1)^2)/(2*((CJ(1,14)^2)-1)))*(((CJ(1,1)/
   soundspeed_fr(gas1))-(1/(CJ(1,1)/soundspeed_fr(gas1))))^2);
Term_1b = (q_h)/(cp_mass(gas1)*T1);
Term_2b = (P_a/P1).^((CJ(1,14)-1)/CJ(1,14));
Term_3b = (P1/CJ(1,2)).^((CJ(1,14)-1)/CJ(1,14));
Term_4b = (CJ(1,3)/T1);
Thrust = GeometryPredictor{CellCorr2Use-GeometryRule,'Mass Flow Rate
   kg/s'}*(sqrt(2*cp_mass(gas1)*T1))*(sqrt(1 + Term_1b - Term_2b *
   Term_3b * Term_4b));

SpecThrust = Thrust/GeometryPredictor{CellCorr2Use-GeometryRule,'Mass
   Flow Rate kg/s'};
ISP = Thrust/(GeometryPredictor{CellCorr2Use-GeometryRule,'Mass Flow
   Rate kg/s'}*9.81);

%% Shak's Playground
Thrust_Goal = 1350; %[N]

m_dot_T = Thrust_Goal / ((sqrt(2*cp_mass(gas1)*T1)) * (sqrt(1 +
   Term_1b - Term_2b * Term_3b * Term_4b))); %[kg/s]

m_dot_V = GeometryPredictor{CellCorr2Use-GeometryRule,'MinFillHeight'
   }*GeometryPredictor{CellCorr2Use-GeometryRule,'MinChannelWidth'}*
   density(gas1)*CJ(1,1); %[kg/s]

Misc=table(Wave_Number_Sean,Mean_Channel_Diam,Fill_Time_Sean,Thrust,
   SpecThrust,ISP,Thrust_Goal,m_dot_T,m_dot_V);
```

C.2 Analytical Model Printout

```
% The new analytical model
% DETechnologies
% Logan and Shak - 2023/2024
```

```
close all force
clear
clc

%% init params
P1 = 130e+3; % [Pa]
T1 = 300;% [K]
eq = 1.0;
mechFiles={'Burke2012.yaml';'h2o2.yaml';'Hong2011.yaml'};
mech = mechFiles{1}; %1 means it uses the first one (burke) (first row
    (row matrix))

%% Call function that does the actual maths
[gas1,vN_Point,CJ,ZND,CellSizePredictions,Misc,GeometryPredictor] =
    NewAnalyticalModel(P1,T1,eq,mech,0,4,1,1);
% % % % % % % % -5 < Bykovskii_adder < 5
% % % % % % % % CellCorr2Use one of these NUMBERS {'Gavrikov','
    Westbrook','Ng','SeanCB'} = 1,2,3,4
% % % % % % % % Geometry rule; 0 = nair, 1 = bykovskii.
% % % % % % % % Print things 1/0

%% Printout Section - for shak

%printing initial state things here.
fprintf('\n\nInitial State')
fprintf('\nPressure: %d [Pa]',P1); fprintf('\nTemperature: %d [K]',T1)
    ; fprintf('\nEquivalence Ratio: %d',eq)
fprintf('\nDensity (initial): %d [kg/m3]',density(gas1)); fprintf('\
    nEnthalpy: %d [kJ/kg]',density(gas1));
fprintf('\nSpeed of Sound (premixed propellant): %d',soundspeed_fr(
    gas1));

%printing out geometry table
fprintf('\n\nGeometry')
GeometryPredictor%dont hide output (no semicolon!!)

%Printing thrust
fprintf('\n\nPerformance Indicators')
fprintf('\nThrust: %d [N]',Misc{1,"Thrust"})
fprintf('\nSpecific Impulse: %d [s^-1]',Misc{1,"ISP"})
fprintf('\nFill Time: %d [s]',Misc{1,"Fill_Time_Sean"})
fprintf('\nWave Number: %d',Misc{1,"Wave_Number_Sean"})
fprintf('\nThrust Goal: %d [N]', Misc{1,"Thrust_Goal"})

%Printing mass flow rate
fprintf('\n\nMass Flow')
fprintf('\nThrust Based Mass Flow: %d [kg/s]', Misc{1,"m_dot_T"})
fprintf('\nChamber Volume Mass Flow: %d [kg/s]', Misc{1,"m_dot_V"})
```

C.3 Analytical Model Calculator

```
% The new analytical model
% DETechnologies
% Logan and Shak - 2023/2024

close all force
```

```
clear
clc

mechFiles={'Burke2012.yaml';'h2o2.yaml';'Hong2011.yaml'};
mech = mechFiles{1}; %1 means it uses the first one (burke) (first row
    (row matrix))

Pressure_range=[0.1*101.325e+3,10*101.325e+3,1e+3]; % low,high,step
   size [Pa]
Temp_range=[300,300,1]; % low,high,step size [K]
eqv_ratio_range=[1,1,0.05];  % low,high,step size
CellSizeCorrelationIndex = 4;
GeometryCorrelationIndex = 0;


CellSizeCorrelations={'Gavrikov','Westbrook','Ng','SeanCB'}; %[1-4]
GeometryCorrelations={'Ng','Bykovskii'}; %[0-1]
n=0;
Outputs=array2table(zeros(0,19),'VariableNames',{'I/P Pressure (Pa)','
   I/P Temperature (K)','Eqv Ratio','I/P Density (kg/m^3)','Speed of
   Sound in Propellant (m/s)',...
                                         'CJ Speed (m/s)','VN Pressure
                                            (Pa)','CJ Temperature (K)',
                                            'CJ Pressure (Pa)','Chosen
                                            Cell Size Correlation',...
                                         'Cell Size value (m)','
                                            WaveNumber','Thrust O/P (N)
                                            ','ISP (s^-1)','mDot (kg/s)
                                            ','Gav Cell Size (m)','
                                            Westbrook Cell Size (m)','
                                            NG Cell Size (m)','SeanCB
                                            cell Size (m)'});
for P1=Pressure_range(1,1):Pressure_range(1,3):Pressure_range(1,2)
    for T1=Temp_range(1,1):Temp_range(1,3):Temp_range(1,2)
        for eq=eqv_ratio_range(1,1):eqv_ratio_range(1,3):
            eqv_ratio_range(1,2)
             n=n+1;
             [gas1,VN,CJ,ZND,CellSizePredictions,Misc,GeometryPredictor
                ] = NewAnalyticalModel(P1,T1,eq,mech,0,
                CellSizeCorrelationIndex,GeometryCorrelationIndex,0);

             %make a table of the things we actually care about here.
             current=[P1,T1,eq,density(gas1),soundspeed_fr(gas1),CJ(1),
                VN(2),CJ(3),CJ(2),{sprintf('%s using %s',
                CellSizeCorrelations{CellSizeCorrelationIndex},
                GeometryCorrelations{GeometryCorrelationIndex+1})},...
                       GeometryPredictor{CellSizeCorrelationIndex*2-
                          GeometryCorrelationIndex,'CellSize'},Misc{1,'
                          Wave_Number_Sean'},Misc{1,'Thrust'},Misc{1,"
                          ISP"},GeometryPredictor{
                          CellSizeCorrelationIndex*2-
                          GeometryCorrelationIndex,'Mass Flow Rate kg/s'
                          },...
                       GeometryPredictor{1*2-GeometryCorrelationIndex,'
                          CellSize'},GeometryPredictor{2*2-
                          GeometryCorrelationIndex,'CellSize'},
```

```
                        GeometryPredictor{3*2-GeometryCorrelationIndex
                        ,'CellSize'},GeometryPredictor{4*2-
                        GeometryCorrelationIndex,'CellSize'}];

            Outputs=[Outputs;current];
            if ~ mod(n,10) %save o/p every n loops so its fast, but
               that we dont lose too much data when errors.
                save('PlottingNice/
                   AnalyticalModel_calculatorOutput_vPressure_March7_fixed
                   .mat','Outputs')
                fprintf('loop number: %d',n)
            end
        end
    end
end
```

C.4 Choked Injector Starting Point

```
% DETechnologies - 2024
% Logan Palmer

%% Housekeeping
close all force
clear
clc

%% Initialize Params
% geometry
OD=60e-3;
Delta=5e-3;
ID=OD-2*Delta;

AnnulusArea=(pi()/4)*(OD^2-ID^2);
m_dot=0.33472; % g/s total

% mass flow rate of propellant
h_massFrac=0.11191;
O_massFrac=1-h_massFrac;
m_dot_h=m_dot*h_massFrac;
m_dot_O=m_dot*O_massFrac;

% chemical properties
gamma=1.4013789;
R_O=259.84; % gas constant O
R_H=4124.2; % gas constant H
T_t=293; % K assume constant temp


%% init desired params
CombutionInitPressure=130e+3;
PlenumDesired=1.89*CombutionInitPressure*3;

e=0.5e+3;
stepsize=1e-4;

% starting point A_i/A_a:
AreaRatio_O=0.17;
```

```
AreaRatio_H=0.06;

%% start iterator
iterator=1

loopNum=0; %init couter.
if iterator
    while true %for oxygen first.
        OxyInjectorArea=AnnulusArea*AreaRatio_O;
        P_upstream_O=(m_dot_O*sqrt(T_t)/OxyInjectorArea)*sqrt(R_O/
           gamma)*(((gamma+1)/2)^((gamma+1)/(2*(gamma-1))));

        if abs(P_upstream_O - PlenumDesired) < e
            %jump out!!!
            break
        else
            if (P_upstream_O - PlenumDesired) > e
                AreaRatio_O=AreaRatio_O+stepsize;
            elseif (P_upstream_O - PlenumDesired) < -e
                AreaRatio_O=AreaRatio_O-stepsize;
            end
        end
        loopNum=loopNum+1;
        fprintf('\n \nloop number: %d',loopNum)
    end
    % print results
    fprintf('\nOxygen Plenum Pressure, %d',P_upstream_O)
    fprintf('\nOxygen Injection Area Ratio, %d',AreaRatio_O)
    fprintf('\nOxygen Injection Area [m^3], %d',OxyInjectorArea)

    % NOW REPEAT THE SAME THING FOR HYDROGEN

    loopNum=0; % reset counter.
    fprintf('\n \nloop number: %d',loopNum)
    while true
        HydroInjectorArea=AnnulusArea*AreaRatio_H;
        P_upstream_H=(m_dot_h*sqrt(T_t)/HydroInjectorArea)*sqrt(R_H/
           gamma)*(((gamma+1)/2)^((gamma+1)/(2*(gamma-1))));

        if abs(P_upstream_H - PlenumDesired) < e
            %jump out!!!
            break
        else
            if (P_upstream_H - PlenumDesired) > e
                AreaRatio_H=AreaRatio_H+stepsize;
            elseif (P_upstream_H - PlenumDesired) < -e
                AreaRatio_H=AreaRatio_H-stepsize;
            end
        end
        loopNum=loopNum+1;
        fprintf('\n \nloop number: %d',loopNum)
    end
    % print results
    fprintf('\nHydrogen Plenum Pressure, %d',P_upstream_H)
    fprintf('\nHydrogen Injection Area Ratio, %d',AreaRatio_H)
    fprintf('\nHydrogen Injection Area [m^3], %d',HydroInjectorArea)
```

```
end

% Print All Results
fprintf('\n\n\n\nSummary')
fprintf('\nOxygen Plenum Pressure, %d',P_upstream_O)
fprintf('\nOxygen Injection Area Ratio, %d',AreaRatio_O)
fprintf('\nOxygen Injection Area [m^3], %d',OxyInjectorArea)
fprintf('\nHydrogen Plenum Pressure, %d',P_upstream_H)
fprintf('\nHydrogen Injection Area Ratio, %d',AreaRatio_H)
fprintf('\nHydrogen Injection Area [m^3], %d',HydroInjectorArea)
```

C.5 Plenum Sizing Based on Real Injection Area

```
% DETechnologies - 2024
% Logan Palmer

%% Housekeeping
close all force
clear
clc

%% Initialize Params
% geometry
OD=60e-3;
Delta=5e-3;
ID=OD-2*Delta;

AnnulusArea=(pi()/4)*(OD^2-ID^2);
m_dot=0.33472; % g/s total

% mass flow rate of propellant
h_massFrac=0.11191;
O_massFrac=1-h_massFrac;
m_dot_h=m_dot*h_massFrac;
m_dot_O=m_dot*O_massFrac;

% chemical properties
gamma=1.4013789;
R_O=259.84; % gas constant O
R_H=4124.2; % gas constant H
T_t=293; % K assume constant temp

%% Init Actual Injection Areas based on DFMA / Physical Constraints
OxyInjectorArea=12.2727/100;
HydroInjectorArea=5.4545/100;

%% Calculate Req'd Upstream Pressure
P_upstream_O=(m_dot_O*sqrt(T_t)/OxyInjectorArea)*sqrt(R_O/gamma)*(((
    gamma+1)/2)^((gamma+1)/(2*(gamma-1))));
P_upstream_H=(m_dot_h*sqrt(T_t)/HydroInjectorArea)*sqrt(R_H/gamma)*(((
    gamma+1)/2)^((gamma+1)/(2*(gamma-1))));

% summary
fprintf('Summary')
fprintf("\nP_upstream_O: %f kPa",P_upstream_O)
fprintf("\nP_upstream_H: %f kPa",P_upstream_H)
```